



UiT The Arctic University of Norway

Department of Electrical Engineering

Wide Area Control and Improvement of Dynamical State of Power System

Phasor Measurement Unit (PMU) Placement on Transmission Networks to Optimize Observability and Wide Area Control (WAC) Implementation

Afshin Nazari

Master's thesis in Electrical Engineering, ELE-3900-1 24V, May 2024

Table of Contents

1	Introduction	1
1.1	Background.....	1
1.2	Problem Description	1
1.3	Project Scopes and Objectives.....	2
1.4	Thesis Outline.....	3
2	Literature Review	4
2.1	A review at historical developments.....	4
2.2	Pahsor Measurement units (PMUs).....	4
2.3	Reviw of existing literature on the placement of PMUs	8
2.4	Literature review on dynamic states of power system and wide area control.....	11
3	Optimal PMU Placement Problem.....	13
3.1	Compelete Observability	13
3.2	Inompelete Observability	14
3.3	Zero Injection Bus (ZIB) Concept.....	15
3.4	Connectivity Matrix Algorithm (CMA)	16
3.5	Testing for Validation.....	21
4	Wide Area Control (WAC) Strategy	26
4.1	Classification of Power system stability.....	26
4.1.1	Rotor Angle Stability	27
4.1.2	Small Signal Stability	27
4.2	Power System Dynamic Analysis Toolbox (PSDAT).....	27
4.2.1	PSDAT capabilities.....	28
4.3	System Modeling	29
4.3.1	Synchronous Generator.....	30
4.3.2	Excitation System.....	30
4.3.3	Turbine System.....	30

4.3.4	Algebraic Equations (Stator and Power Flow).....	31
4.3.5	Load Model.....	31
4.3.6	Reference Angle.....	32
4.3.7	Initial Conditions Calculation.....	32
4.4	Model Analysis.....	33
4.4.1	Eigenvalue, Eigenvector, Damping Ratio, and Frequency	34
4.4.2	Mode Shape	34
4.5	Frequency Response Analysis	34
4.6	Simulation Results (without Controller).....	35
4.6.1	Tie-line Scenario Analysis	35
4.6.2	Branch Data Scenario Analysis.....	38
4.6.3	Power System Integrated with a Renewable energy Resource (RES) Scenario Analysis	40
4.7	Model-Based and Model-Free Control in Power Systems	42
4.8	Test System with presence of the controller.....	42
4.9	Scheme for Reinforcement Learning (RL) Control.....	43
4.9.1	RL Setup	44
4.9.1.1	RL agent setup	44
4.9.1.2	Environment setup	45
4.10	Simulation Results (With RL Controller).....	45
5	Conclusion and Recommendation for Future Work	47
5.1	Summary of key Findings.....	47
5.2	Limitations and Challenges	47
5.3	Recommendation for Future Work.....	48
	References.....	49

List of Tables

Table 1- Optimal PMU placement results without ZIB in different IEEE bus systems	21
Table 2- Optimal PMU placement results with consideration of ZIB in different IEEE bus systems.....	23
Table 3- Parameters and variables for synchronous generator dynamics and control	29
Table 4- Tie-lines analysis with total inter-tie flows and convergence time in various IEEE-9bus configurations	35

List of Figures

Figure 1- Basic PMU block diagram.....	5
Figure 2- Deployment of the PMUs in the North American grid between 2009 and 2014	6
Figure 3- Deployment of the PMUs in the Swiss.....	6
Figure 4- State estimation vs. PMU measurements	7
Figure 5- Example of a bus system that is fully observable.....	13
Figure 6- Depth of one unobservability illustrated	14
Figure 7- Depth of two unobservability illustrated	15
Figure 8- IEEE-14 bus test system single line diagram and its connectivity matrix	17
Figure 9- ZIB implementation rule number 1	18
Figure 10- ZIB implementation rule number 2	18
Figure 11- ZIB implementation rule number 3	19
Figure 12- ZIB implementation rule number 4	19
Figure 13- ZIB implementation rule number 5	19
Figure 14- CMA's matrix format	20
Figure 15- IEEE-9 bus system (without considering ZIB), 3 PMUs	22
Figure 16- IEEE-14 bus system (without considering ZIB), 4 PMUs	22
Figure 17- IEEE-9 bus system (with considering ZIB), 3 PMUs	24
Figure 18- IEEE-14 bus system (with considering ZIB), 3 PMUs	24
Figure 19- Types of power system stability	26
Figure 20- Visualisations of the mode shape for rotor speed state variables and lightly damped modes of IEEE-9 bus systems (One-area, Two-area, Three-area).....	36
Figure 21- Frequency response analysis: Nichols's plot (left) and Bode plot (right) of all systems (One-area, Two-area, Three-area)	37
Figure 22- Pole-zero map of all the systems (One-area, Two-area, Three-area).....	37

Figure 23- Two-area IEEE-9 bus test system.....	38
Figure 24- Mode shapes plots without controller.....	39
Figure 25- Pole-zero map of the system without controller.....	39
Figure 26- Two-area IEEE-9 bus test system (with G1 replaced by a PV plant)	40
Figure 27- Mode shapes plots without controller (with G1 replaced by a PV plant)	41
Figure 28- Pole-zero map of the system without controller (with G1 replaced by a PV plant)	41
Figure 29- Mode shapes plots test system with controller along with integrating PMUs	43
Figure 30- An agent-environment model in Simulink	44
Figure 31- Simulink-based agent-environment control scheme	45
Figure 32- System analysis with RL controller in time domain	46

Acknowledgement

This thesis is a part of UiT-The Arctic University of Norway's Master of Electrical Engineering curriculum in Electrical Engineering.

I would like to express my deepest gratitude to my thesis supervisor, Prof. Charu Sharma, for her invaluable guidance, support, and encouragement throughout this research journey. Her expertise and advice were crucial to the completion of this work.

I would also like to thank Dr. Isaac Kweku Aidoo for his assistance and insights, which significantly contributed to my understanding and progress during this thesis.

I dedicate this thesis to the memory of my late brother, Amir, whose spirit and inspiration continue to drive me. I am grateful for the love and support of my family, who stood by me through thick and thin.

Without the contributions of all these individuals, this thesis would not have been possible. Thank you for being part of this journey with me.

Abstract

Some approaches to achieving full observability and controllability in power systems are explored in this thesis. The core structure of this work consists of observability and controllability, focusing on two key phases of optimization and control.

In the first phase, system observability is addressed through optimal placement of Phasor Measurement Units (PMUs). The Connectivity Matrix Algorithm (CMA) is used to determine the optimal PMU locations, initially without consideration of Zero Injection Buses (ZIBs), and then considering them to ensure full system observability. The transmission system simulation results for the IEEE 9, 14, 24, 30, 57, and 118 bus systems has been shown. MATLAB R2024a is utilized to validate the methodology, providing a robust framework for achieving optimal PMU configuration across different system scales and configurations.

In the second phase, firstly the IEEE-9 bus test system has been used without a controller, testing three different scenarios (tie-line, branch data, and solar plant integration) to assess system stability. Thereafter, a Deep Deterministic Policy Gradient (DDPG) algorithm-based controller is introduced, which is grounded in Reinforcement Learning (RL). In Wide-Area Measurement Systems (WAMS), the controller uses frequency information to receive its global input signal from PMU devices. This method is used to improve controllability and damp out low frequency oscillations in power systems after PMU integration. The development of a Wide Area Control (WAC) strategy for stable power system operations is a key focus of this phase.

Through these objectives, this thesis aims to contribute to the field of power system stability and control by optimizing system observability and implementing effective control strategies to improve dynamic performance. The proposed approaches provide a foundation for future research and practical applications in wide area control and power system dynamics.

1 Introduction

1.1 Background

The complexity of power systems has heightened with the rapid growth in electricity demand, and they are predominantly operated under stressful conditions [1]. This scenario has been a significant contributor to the occurrence of expensive blackouts. To address this issue, the implementation of a real-time Wide-Area Monitoring, Protection and Control System (WAMPACS) is imperative for efficient power system resource management. Wide Area Measurement Systems (WAMS) enables operators to ensure system security and seamless operation. An essential component of the Energy Management System (EMS) is state estimation, which, based on network-wide measurement, provides an estimation of power system state variables while ensuring consistency with the actual measurements. Conventionally, the SCADA (Supervisory Control and Data Acquisition) systems has supplied input measurements. A drawback is the lack of synchronization in these measurements, leading to less accurate state estimation during dynamic events in the network [2]. A PMU is a device that measures the positive sequence voltage and current, employing the Global Positioning Systems (GPS) to synchronize them to a unified time reference [3]. PMUs provide synchrophasor voltage, current, frequency and Rate of Change of Frequency (ROCOF) which results in linear and dynamic State Estimation (SE) models can be implemented. For implement a control strategy effectively in a power system, we need access to data. PMU Placement (which provides information about the system's state) allowing operators to observe and monitor system's behavior.

1.2 Problem Description

The power system's dynamic reaction will get more sophisticated and faster when additional Converter Interfaced Generation (CIG) devices are incorporated. The stability and regulation of the electricity grid face major issues in this future scenario. In order to maintain power system stability and facilitate a smooth transition, we must abandon our current control strategies, which rely on isolated and decentralized local control operations, and start investigating other approaches. Wide Area Control (WAC) is a promising solution to address fundamental stability concerns and control complexity in future low-inertia power systems. With this technology, control is based on a series of coordinated actions over large areas, where interplant communication is crucial, rather than just localized duties.

The introduction of Phasor Measurement Units (PMUs) and Wide Area Measurement Systems (WAMS) represents a major advancement in technology. However, utilizing these tools to fully observe and widely control interconnected power grids remain a considerable challenge. The primary challenges involve optimizing PMU placement for complete observability and developing robust control strategies to mitigate inter-area oscillations and/or low-frequency oscillations along with dynamic instabilities. These oscillations and instabilities have the potential to cause serious power quality problems as well as broad system blackouts if they are not controlled.

1.3 Project Scope and Objectives

One feature of the proposed research approach is that it takes into account scenarios with Zero-Injection Buses (ZIBs) while simultaneously putting PMUs to ensure total system observability even in their absence. Along with addressing PMU placement for full observability, this study also develops a wide area control method that targets low frequency oscillations dampening and ensures system controllability through Reinforcement Learning (RL) method.

As a result, the research objectives are outlined as follows:

- 1- Placement of a fixed number of PMUs in the system, taking into account the absence of ZIBs and considering the presence of ZIBs so as to make system fully-observable.
- 2- Analyzing of IEEE9 bus test system in case of power system stability using Power System Dynamic Analysis Toolbox (PSDAT) in MATLAB R2024a.
- 3- Develop a strategy for implementation of Wide Area Control (WAC) in the system to damping low frequency oscillations using Reinforcement-Learning (RL) phenomena.

1.4 Thesis Outline

This thesis is organized into five main chapters:

Chapter 1 of the thesis represents an overview of the study's background, problem description, and motivations, with a special emphasis on the power system stability issues brought on by the integration of renewable energy sources.

Chapter 2 covers the literature review of the thesis which discusses the technology and applications of PMUs and the history of them, the placement of PMUs in power systems, and the dynamics of power systems in conjunction with Wide Area Control techniques.

Chapter 3 covers the methodology of Connectivity Matrix Algorithm (CMA) for PMU placement, discusses observability criteria, and presents simulation results across various IEEE bus systems.

Chapter 4 focused on the development and simulation of a Reinforcement Learning (RL)- based control strategy. This chapter explains the setup of the RL environment, including the design of the RL agent and the simulation results demonstrating the control strategies effectiveness in stabilizing the IEEE9 bus test power system with integration of a Photovoltaic (PV) plant.

Finally, chapter 5 summarizes the findings, discusses limitations, and suggests future research directions for enhancing power system resilience.

2 Literature Review

2.1 A review at historical developments

Power engineers have long been intrigued by the phase angles of voltage phasors at power system buses. Theoretically, the active (real) power transmitted through a distribution line is directly related to the sine of the angle disparity between voltages at its two terminals. The angle difference is considered a fundamental parameter for assessing the state of the power network.

During the early 1980s, advanced tools for directly measuring the phase angle difference were introduced [4,5]. The clock synchronization method initially involved using the LORAN-C signal, GOES satellite transmission, and HBG radio transmission (in Europe). Subsequently, researchers employed the positive-going zero crossing of a phase voltage to estimate the local phase angle in relation to the time reference. The phase angle difference between voltages at two bus locations was determined by comparing the measured angles to a common reference for both locations. However, the measurement accuracies were around 40 microseconds, proving insufficient for capturing the harmonics in the voltage waveform. Consequently, these methods were not preferred for wide-area phasor measurement systems. As the deployment of GPS satellites increased, researchers recognized the potential of utilizing GPS time signals as an input to the sampling clock. GPS provided timing with an accuracy ranging from 1 nanosecond to 10 nanoseconds [6]. Simultaneously, the GPS receiver has the capability to provide a distinctive pulse signal at one-second intervals, commonly referred to as 1 Pulse Per Second (PPS). Therefore, by integrating a high-precision system into a measuring device, it was evident that this system provided the most efficient method for synchronizing power system measurements across extensive distances. Subsequently, commonly available PMUs incorporating GPS technology were developed, and their implementation commenced in power system globally.

2.2 Phasor Measurement Unit (PMU)

In 1988, Dr. Arun G. Phadke and Dr. James S. Thorp from Virginia Tech introduced Phasor Measurement Unites (PMUs). Figure 1 illustrates a block diagram of a PMU. These devices are capable of measuring 50 or 60 Hz waveform, encompassing voltages and currents, typically at a rate of 48 samples per cycle, equivalent to 2880 samples per second. Initially, anti-aliasing filters are incorporated into the PMU input. These filters introduce a delay, dependent on the signal frequency, due to their specific characteristics. Consequently, the PMU must compensate

for this delay, as the sample data are collected after the introduction of the anti-aliasing delay by filter.

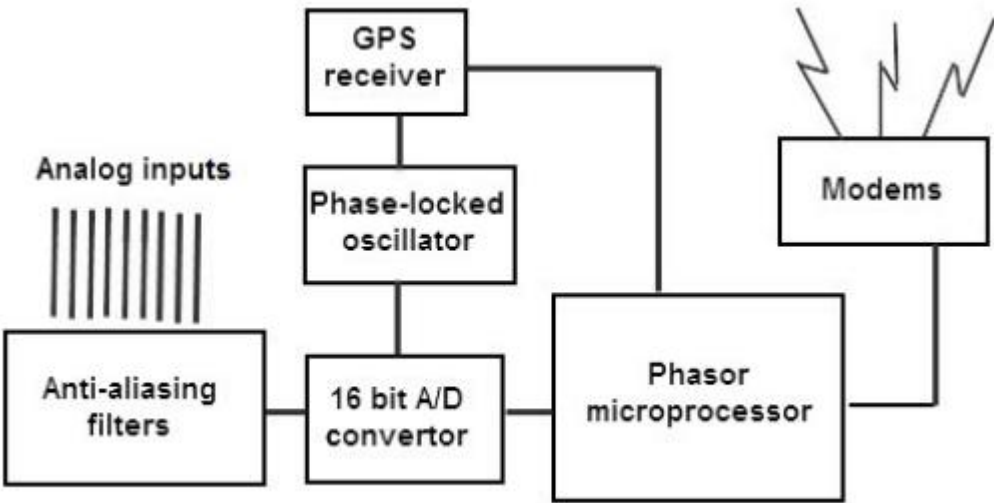


Figure 1 - Basic PMU block diagram [7]

For each phase, the analog AC waveforms undergo digitization through an analog-to-digital converter. To achieve high-speed synchronized sampling with 1-microsecond accuracy, a phase-lock oscillator referencing the Global Positioning System (GPS) is utilized. The captured phasors are then time-tagged based on the Coordinated Universal Time (UTC) frame.

More than 2000 commercial-grade PMUs are currently operational throughout North America, providing real-time condition data to control centers, with the quantity growing annually [8]. Figure 2 illustrates the rise in PMU deployment from 2009 to 2014. According to the North American Synchro-Phasor Initiative (NASPI), the quantity of PMUs installed in the United States and Canada surged nearly ninefold from 2009, with 200 research-grade PMUs, to 2014, boasting 1700 production-grade PMUs [9]. Figure 3 illustrates the locations of the PMUs in the Swiss network. In Europe, PMUs are employed for evaluating the stability of the interconnected European transmission network concerning inter-area oscillation in the North-South and West-East directions [10].

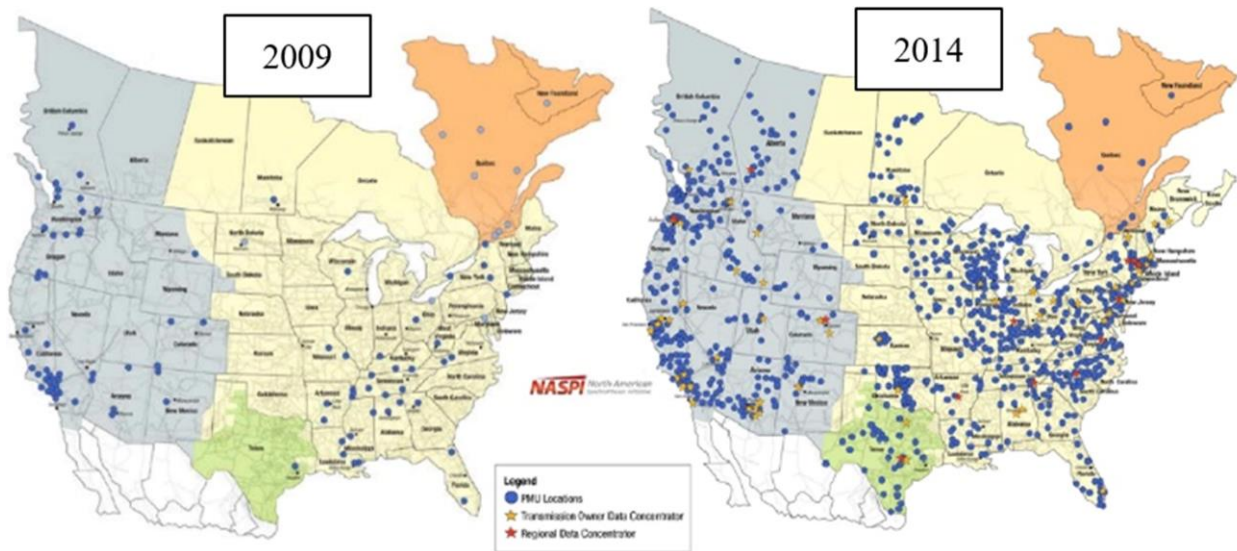


Figure 2- Deployment of the PMUS in the North American grid between 2009 and 2014 [9]

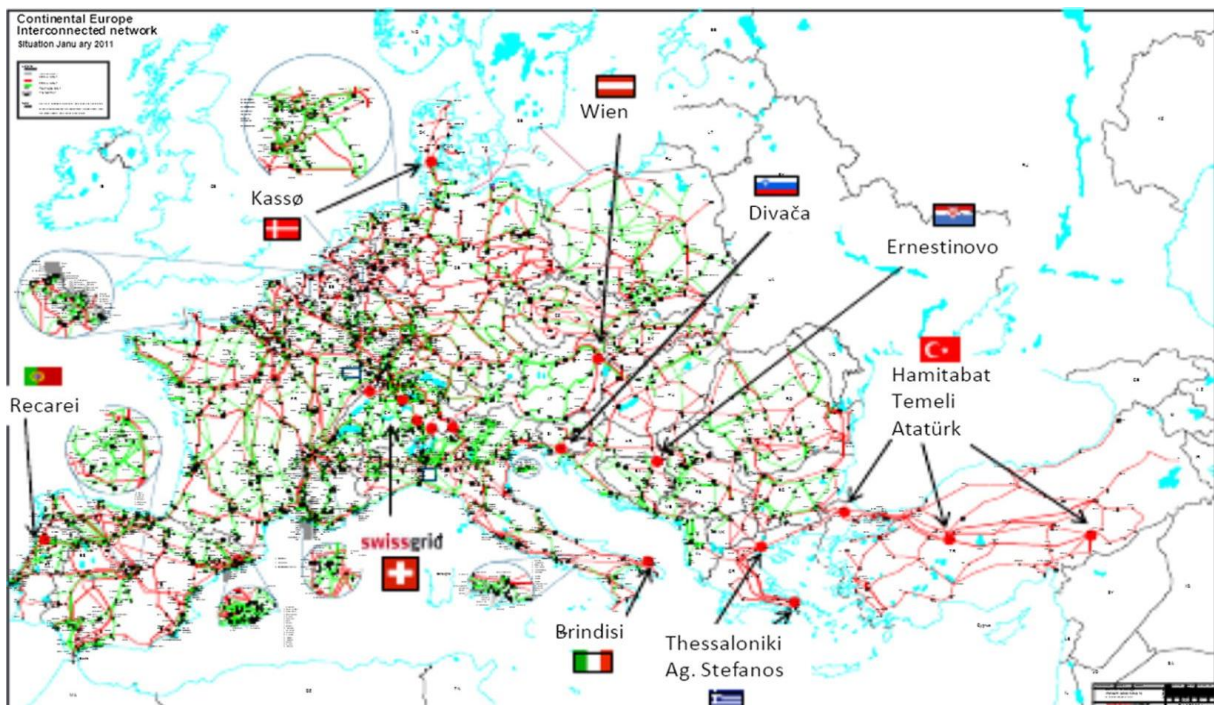


Figure 3 - Deployment of the PMUS in the Swiss Grid [10]

If a sufficient number of PMUs are deployed throughout an extensive power transmission network, they can directly gauge the real-time operational status of the system. Moreover, due to the high data reporting rate of PMUs, they can effectively capture the system's dynamics during disturbances. Figure 4 illustrates the contrast in voltage angle variation between two substations as determined by PMU measurements and conventional state estimation. This

comparison highlights the superior accuracy and real-time insights offered by a monitoring system consisting of PMUs compared to traditional state estimation methods.

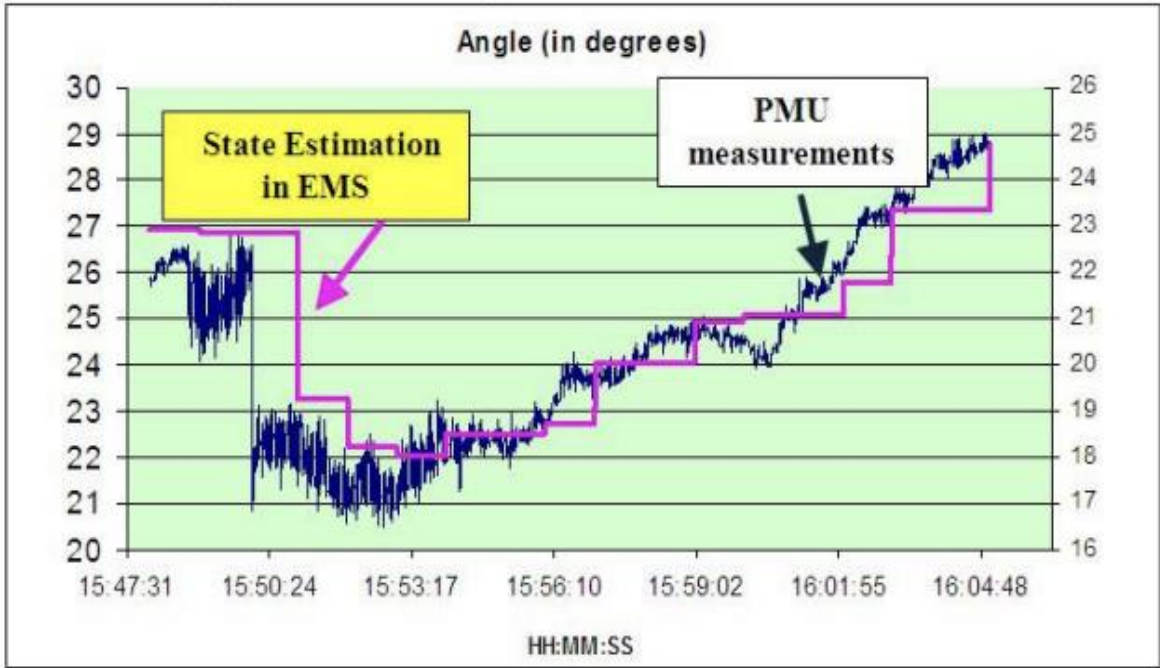


Figure 4 - State estimation vs. PMU measurements [11]

In comparison to the conventional data obtained from the SCADA system, the synchronized PMUs exhibit a data capture speed that is a hundred times faster and offers greater measurement accuracy. SCADA systems operate in a quasi-steady state and are consequently unable to measure transient phenomena. Typically comprised of Remote Terminal Units (RTUs), SCADA systems interface with sensors capable of measuring only magnitude, lacking the ability to capture phasors. The incorporation of PMUs into the system accelerates state estimation processing due to the inherent relationship between PMUs and state variables. A power system is considered observable when the deployed measurements enable the determination of bus voltage magnitude and angle at every bus within the system. System observability estimation involves considerations of network topology, measurements types, and their locations. The direct installation of a PMU at a bus ensures direct observability, as the PMU measures the phasor voltage of that specific bus. Moreover, given that PMUs provide the current phasor of the interconnected branch or line, the adjacent bus becomes indirectly observable. This indirect observability arises from the availability of current phasors, facilitating the estimation or calculation of voltage phasors using line parameters.

2.3 Review of existing literature on the placement of PMUs

The main objective of the state estimator is to determine the optimal estimates of bus voltage phasors, considering available measurements in the system and the network topology. Typically, RTUs at substations provide measurements, including active/reactive power flows, power injections, bus voltage magnitudes, and branch currents. With the widespread availability of commercial PMUs, some utilities and power industries have begun integrating them into their networks, while others plan to incorporate them in the future. The crucial consideration in this context is the cost. Given the relatively high cost associated with PMUs and their installation, planning engineers encounter challenges in determining the optimal locations for placing PMUs. This planning may involve initial deployment or the addition of new PMUs to a network already equipped with some sets of PMUs. As mentioned in the preceding section, the degree of observability in a system is greatly influenced by the quantity of installed PMUs. Given the crucial importance of power systems, it is essential to ensure continuous visibility of every node at all times. The strategic positioning of PMUs has been a crucial subject of investigation in the realm of PMU applications. Despite the diverse uses of PMUs, the exploration and discourse on their placement are exclusively confined to applications related to state estimation and power engineers globally have introduced various methodologies in this regard [12]. The PMU placement problem has been addressed by researchers through two approaches: (1) Heuristic approach and (2) Mathematical approach.

Optimal placement of PMUs with consideration of fault-location topological observability on long transmission lines has been carried out in [13]. The paper suggested two functions for Optimal PMU Placement (OPP) in a practical network, considering cost and fault location capability. It used a Multi-Objective Linear Programming (MOLP) model in General Algebraic Modeling System (GAMS) software with the CPLEX solver on Oman's power network. The solution, obtained through iterative Mixed Integer Linear Programming (MILP), was presented on the Pareto front using the ϵ -constraint method, and a decision-making index called Fault Location Observability (FLO). In [14] the Observability of power systems with optimal PMU placement has been carried out. It presented two mathematical programming models for the PMU Placement Problem (PPP): a single-level and a bilevel integer programming model. To improve both formulations, new valid inequalities, and variable fixing were introduced. For the bilevel model, a cutting plane algorithm was developed with enhanced features for efficiency, as confirmed by computational experiments. Results indicated superior efficiency compared to previous approaches. Characterization and optimization of cyber threats targeting PMU

placement in a smart grid was carried out in [15]. Findings showed that cyber threats significantly increase power system unobservability risk, requiring additional PMU allocations, and interdependence among cyber-attacks can amplify these risks. The researchers of [16] accomplished new and thorough optimal placement of PMUs considering practical aspects in the design and implementation of a Wide-Area Measurement System (WAMS). Besides the traditional elements of the OPP, such as monitoring the system buses, ensuring measurement redundancy, addressing limitations in PMUs channels, and accounting for the zero-injection effect, the proposed method also took into account practical challenges. The suggested framework was developed using a MILP formulation. Simulation results demonstrated the model's effectiveness in addressing practical issues and achieving global minimum PMU costs and numbers. In [17] a method for solving the optimal placement challenge of PMUs to achieve complete observability of power networks, especially during contingencies was proposed. In this research a nonlinear programming-based methodology to solve the optimal PMU positioning problem for total power network observability while taking contingencies into account was presented. The results of this research showed that the suggested procedure is easy to implement, and in certain situations, there is a reduction in the required minimum number of PMUs. Haggi et al. [18] investigated a formulated Multi Objective Resilient PMU Placement (MORPP) problem, and solved it with a Modified Teaching-Learning-Based Optimization (MO-TLBO) algorithm. Three objectives were considered in the MORPP problem, minimizing the number of PMUs, maximizing the system observability, and minimizing the voltage stability index. A method for optimizing the placement of PMUs, considering costs and risk assessments of state estimation, was introduced in [19]. Initially, the researchers in [19] presented a multi-objective model to optimize the placement of PMUs. Subsequently, they categorized the buses using the Jacobi matrix and grid structure and assessed the unobservable risk probability of the system by estimating the state of PMUs on the buses, aiming to achieve system observability. Finally, the placement schemes were determined by solving the non-dominated Pareto solution sets using the Non-dominated Sorting Genetic Algorithm (NSGA-II). The investigation involved analyzing the time delay in a Wide Area Monitoring and Control System (WAMCS) when addressing grid contingencies was carried out in [20]. In this study, flexible AC transmission system devices were deployed and managed through a Wide Area Controller (WAC). In [21] cyber-physical resilience for Wide-Area Monitoring, Protection, and Control (WAMPC) in the power grid has been carried out. This paper made three key contributions to enhancing WAMPC cybersecurity and resilience. Firstly, it proposed an end-to-end attack-resilient cyber-physical security framework for WAMPC applications in the

power grid, covering the entire security life cycle. Secondly, it introduced a defense-in-depth architecture integrating attack resilience at both infrastructure and application layers. Thirdly, it highlighted critical research issues and presented attack-resilient algorithms, providing insights and paving the way for future research in this field. In [22], the literature proposes an exhaustive search approach for contingency-constrained optimal PMU placement. This study takes into consideration several zero-injection buses for PMU placement, taking into account single PMU loss and limitations in measurement channels. In [23], a MILP approach is utilized, considering both zero injection and branch flow measurements to maximize measurement redundancy and minimize the number of required PMUs. However, it is noted that the approach in [23] necessitates nearly twice the number of PMUs to achieve full system observability during contingency operations compared to normal operating conditions. In [24], a three-stage OPP technique based on a topology matrix is provided. The most crucial buses, where the algorithm is certain that the PMU is significant, and the less important buses, where the PMU might not be required, are defined in the first two stages. Following the third round of pruning, the best location for the PMU should be determined. The technique also addresses the N-1 criterion and has been verified for the following IEEE test systems: 14-bus, 24-bus, 30-bus, 57-bus, and 118-bus. The dependability of ZI observation is taken into consideration when proposing a unified PMU placement model in [25]. In this study, two trustworthy metrics—the depth of ZI observation and the zero-injection utilization rate—are defined for ZIBs, which are modeled in the OPP, a novel pattern. The best location is chosen in order to minimize the two preceding parameters. The N-1 criterion for each of the several redundancy scenarios are also included in the method.

2.4 Literature review on dynamic states of power system and wide area control

In [26] Ismael Abdulrahman, has been proposed a solar PV plant damping control strategy through Reinforcement-Learning (RL) based using Deep Deterministic Policy Gradient (DDPG) algorithm in a Wide-Area Measuring System (WAMS). In this paper Using frequency data, the controller obtains its input data from PMUs in WAMS. Time-domain simulation, frequency response analysis, pole-zero maps, and participation factor map were used in its study, in MATLAB software. The architecture takes communication latency into consideration, resulting in improved dampening of inter-area oscillations and increased system stability. In [27] Twin-Delayed Deep Deterministic (TD3) Policy Gradient for low-frequency oscillation damping control has been carried out. The paper proposed a novel reward algorithm, taking into account the machine speed deviation, the episode termination prevention, and the feedback from the action spaces. The method showed a fast-learning curve and good control performance under varying communication latency. In [28], by using a wide-area solar plant with adaptive time-delay correction, power oscillations were dampened. The area phase-angle difference, linked closely to active power flow and system stress monitoring, was used as the controller's remote signal input, obtained via PMUs and WAMS. To manage variable signal delays, an adaptive compensator employing a neuro-fuzzy inference system was developed. Using a two-area four-machine test system and a custom Simulink package, the study's simulations showed the controller's effectiveness in damping inter-area oscillations across various disturbances and time delays.

In order to address system observability and low-frequency oscillations, comprehensive techniques that combine optimal PMU placement with efficient control strategies are still required, despite notable advancements in PMU placement and Wide Area Control (WAC) strategies covered in the literature. This thesis aims to bridge the gap by integrating effective PMU placement with sophisticated control strategies to increase power system stability. The majority of the literature to date has examined Wide Area Control (WAC) and Phasor Measurement Unit (PMU) placement as separate and independent research topics.

The methodology employed in this thesis is structured into two primary stages:

- 1- In the initial stage, the optimal PMU placement is determined using the Connectivity Matrix Algorithm (CMA). This placement is tested both with and without considering Zero Injection Buses (ZIBs) to obtain full system observability. The efficacy of the CMA is demonstrated across a variety of test systems including IEEE-9, IEEE-14, IEEE-24, IEEE-30, IEEE-57, and IEEE-118 verifying the adaptability and wide-ranging use of the algorithm.

- 2- The second stage focuses on enhancing system stability and controllability using the IEEE-9 bus test system as a model. Initially, the system is assessed without any controllers under three distinct scenarios: tie-line adjustments, branch data modifications, and the integration of a solar plant with the test system. Following these assessments, a Deep Deterministic Policy Gradient (DDPG) strategy, based on Reinforcement Learning (RL), is proposed. This approach is specifically designed to dampen low-frequency oscillations and enhance the overall controllability of the power system.

3. Optimization PMU Placement (OPP) Problem

Installing PMUs at every bus in a power system allows direct state measurement but is expensive. By measuring line currents, voltage measurements can be extended to buses without PMUs. This way, a minimal number of PMUs can be used to indirectly measure all bus voltages. The challenge is to determine the optimal number and location of PMUs for effective system monitoring. In this thesis the methods discussed in [29] and [30] were used.

3.1 Complete Observability

PMUs can measure phasor voltages and currents immediately at various geographic locations when used as a synchro-phasor measurement instrument. Thus, in the event that a PMU is installed at a typical bus, the PMU will directly measure the phasor voltage at that bus as well as the phasor currents in all related lines. However, if a PMU is placed at a bus, it is possible to compute the phasor voltage at the adjacent buses using Ohm's law. A system that is entirely observed by two PMUs (big circles) is shown in Figure 5. The smaller circles' shade reveals which PMU gives the nearby buses observability.

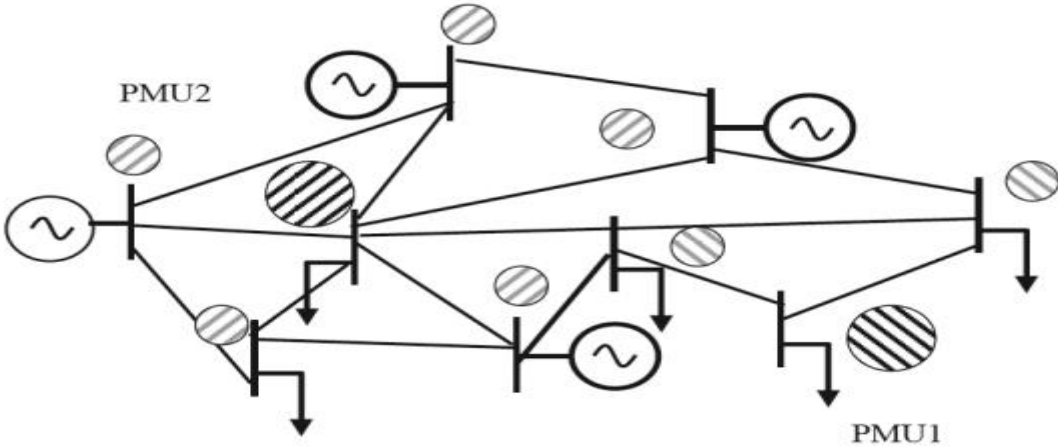


Figure 5- Example of a bus system that is fully observable [4]

To solve the placement problem for complete observability, the minimum possible number of PMUs must be identified so that a PMU reaches every bus at least once [31].

3.2 Incomplete Observability

When the quantity and placement of PMUs are insufficient to ascertain the full set of bus voltages of a power system, the situation known as incomplete observability arises. An incompletely observed system is depicted in Figure 6. While the voltages at buses A, C, E, and G can be computed using the observed voltages and line currents, the voltages at buses B and F are directly measured by PMU-1 and PMU-2, respectively. Bus D is now considered unobservable. Bus voltages and line currents are measured directly on buses B and F, which we designate as PMU buses. Since the voltages of the buses that are connected to A, C, E, and G are determined from the PMU measurements of those buses, we refer to those buses as calculated buses. Moreover, we characterize this configuration as a system with unobservability at depth of one. In other words, two or more computed buses are connected to a single unobserved bus. There will be a depth-of-two unobservability if PMU-2 is moved to bus G (Figure 7); buses D and E are the two unobserved buses that are positioned between the computed buses. Next, utilizing the computed and observed buses, the voltages at the unobserved buses are estimated.

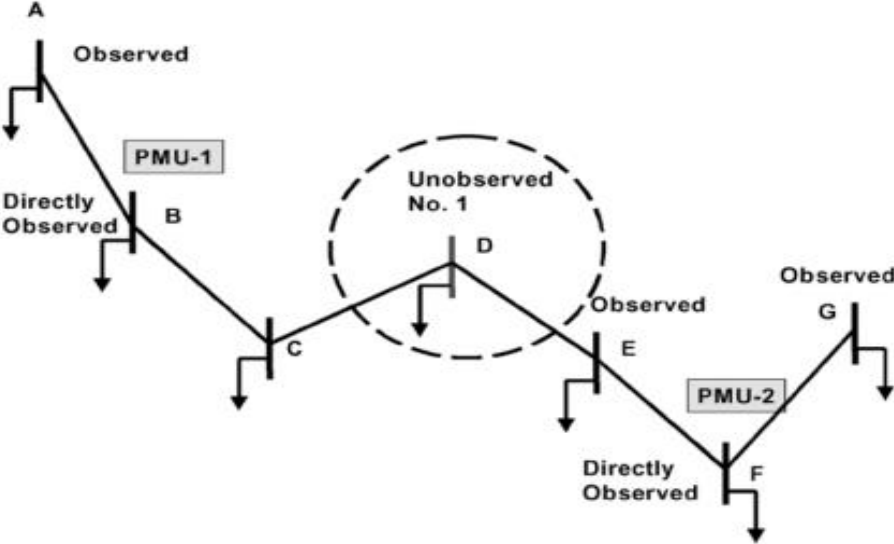


Figure6. Depth of one unobservability illustrated [32]

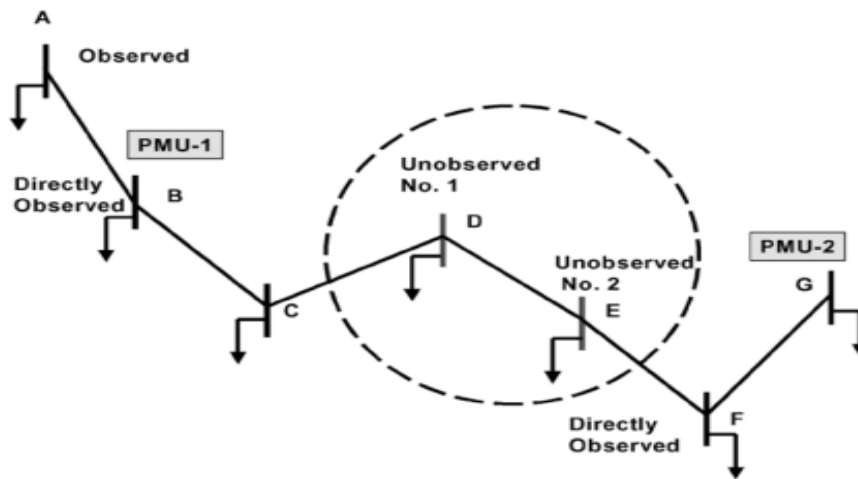


Figure 7 - Depth of two unobservability illustrated [32]

3.3 Zero Injection Bus (ZIB) Concept

Zero Injection Bus (ZIB) refers to any bus in the system that is not in use for generation or load. There are two more indirect strategies that can be used with these buses. The first one is based on nodal analysis, which allows for the computation of the ZIB phasor voltage as all connected buses are visible. Ohm's law and Kirchhoff's Current Law (KCL) are the foundations of the second method. This technique allows the voltage of the unobservable bus to be calculated if ZIB and all associated buses, with the exception of one, are observable. The OPP problem has more flexibility in its solution thanks to these two exceptions [30].

Without taking ZIBs into account, there are a few important considerations when placing PMUs. First, the fact that ZIBs are not evenly dispersed across the electrical system draws attention to the limited coverage, which may leave important regions unmonitored. The second point that is brought up is cost, specifically that the additional hardware and infrastructure needed to deploy PMUs at ZIBs may result in higher expenses than advantages. However, there are a few benefits to placing PMUs when taking ZIBs into account. It emphasizes three main advantages:

- 1- **Strategic Locations:** which emphasize the significance of monitoring critical areas like tie lines, grid interconnections, and voltage regulation zones for stability and control.
- 2- **Wide-Area Monitoring:** which enables operators to use synchronized measurements for comprehensive oversight and response to large-scale disturbances across regions.

- 3- **Enhanced Observability:** which allows PMUs to provide additional system insights without being affected by local generation or load conditions.

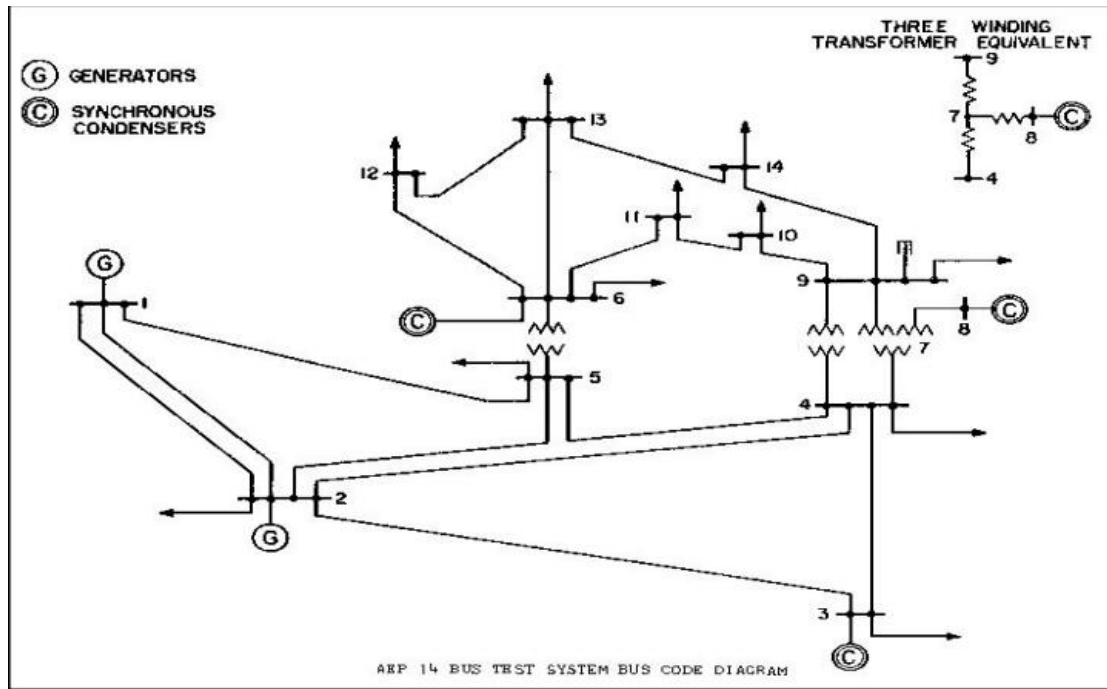
The optimization problem known as Optimal PMU Placement (OPP) aims to determine the minimum number of PMUs required for the system to be fully observable.

3.4 Connectivity Matrix Algorithm (CMA)

The system's connectivity matrix, also known as the topology matrix, serves as the foundation for this simple algorithm. Any system's connectivity matrix can be determined by looking at its topology in the following way:

- The size of the connectivity matrix is $(n \times n)$, where n is the number of system nodes (Busbars).
- The connectivity matrix's primary diagonal elements are always ones.
- The connections between the nodes are represented by the off-diagonal elements; if the i^{th} and j^{th} nodes are connected (directly), the ij element in the connectivity matrix is one; if not, it is zero.

Considering the concept of the connectivity matrix, Figure8 depicts the IEEE-14 bus test system. It shows the electrical network's single line configuration, which includes transformers, generators, synchronous condensers, and load connections, as well as its corresponding connectivity matrix (D), where '0' denotes no direct connection and '1' indicates the presence of a direct line between buses.



$$D = \begin{bmatrix} 1 & 1 & 0 & 0 & 1 & 0 & 0 & 0 & 0 & 0 & 0 & 0 & 0 & 0 \\ 1 & 1 & 1 & 1 & 1 & 0 & 0 & 0 & 0 & 0 & 0 & 0 & 0 & 0 \\ 0 & 1 & 1 & 1 & 0 & 0 & 0 & 0 & 0 & 0 & 0 & 0 & 0 & 0 \\ 0 & 1 & 1 & 1 & 1 & 0 & 1 & 0 & 1 & 0 & 0 & 0 & 0 & 0 \\ 1 & 1 & 0 & 1 & 1 & 1 & 0 & 0 & 0 & 0 & 0 & 0 & 0 & 0 \\ 0 & 0 & 0 & 0 & 1 & 1 & 0 & 0 & 0 & 0 & 1 & 1 & 1 & 0 \\ 0 & 0 & 0 & 1 & 0 & 0 & 1 & 1 & 1 & 0 & 0 & 0 & 0 & 0 \\ 0 & 0 & 0 & 0 & 0 & 0 & 1 & 1 & 0 & 0 & 0 & 0 & 0 & 0 \\ 0 & 0 & 0 & 1 & 0 & 0 & 1 & 0 & 1 & 1 & 0 & 0 & 0 & 1 \\ 0 & 0 & 0 & 0 & 0 & 0 & 0 & 0 & 1 & 1 & 1 & 0 & 0 & 0 \\ 0 & 0 & 0 & 0 & 0 & 1 & 0 & 0 & 0 & 1 & 1 & 0 & 0 & 0 \\ 0 & 0 & 0 & 0 & 0 & 1 & 0 & 0 & 0 & 0 & 0 & 1 & 1 & 0 \\ 0 & 0 & 0 & 0 & 0 & 1 & 0 & 0 & 0 & 0 & 0 & 1 & 1 & 1 \\ 0 & 0 & 0 & 0 & 0 & 0 & 0 & 0 & 1 & 0 & 0 & 0 & 1 & 1 \end{bmatrix}$$

Figure 8- IEEE-14 bus test system single line diagram and its connectivity matrix [29]

As previously mentioned, ZIBs are defined as any bus that has no load or generation. Here is a summary of the main idea behind system observability:

- All nodes connected to an i^{th} node as well as the i^{th} node itself are observable (direct observability) if a PMU is deployed at that node.
- Nodal analysis can be used to determine the non-observable bus voltage if the ZIB and every bus connected to it are observed, with the exception of one.

Figures 9 through 13 illustrate the stages of ZIB implementation. The Connectedly Matrix Algorithm (CMA) [29],[30] which is based on the topology network of a power system implements the ZIB as follows which include five rules:

- 1- A ZIB-related bus gets eliminated from the system if it has just one connection.

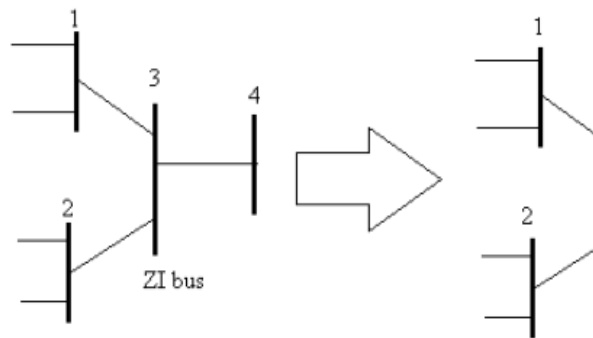


Figure 9- ZIB implementation rule number 1

- 2- The ZIB is eliminated if it only has two connections.

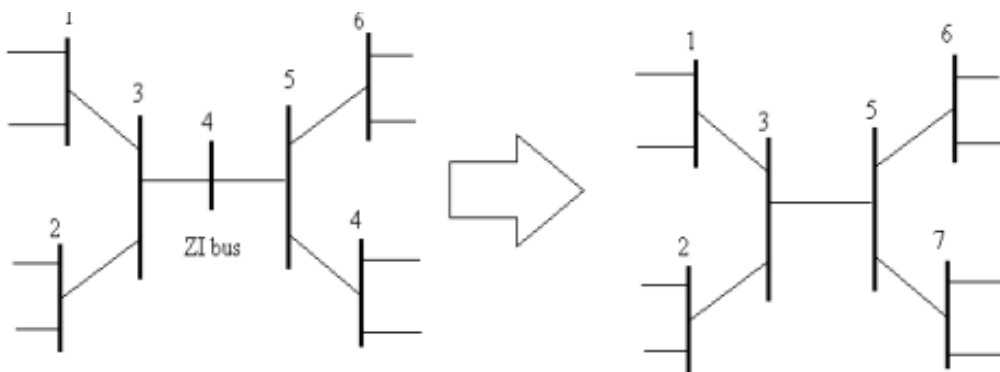


Figure 10- ZIB implementation rule number 2

- 3- In the case that the ZIB has three connections, it is removed and the two connected buses that have the fewest connections need to be rejoined.

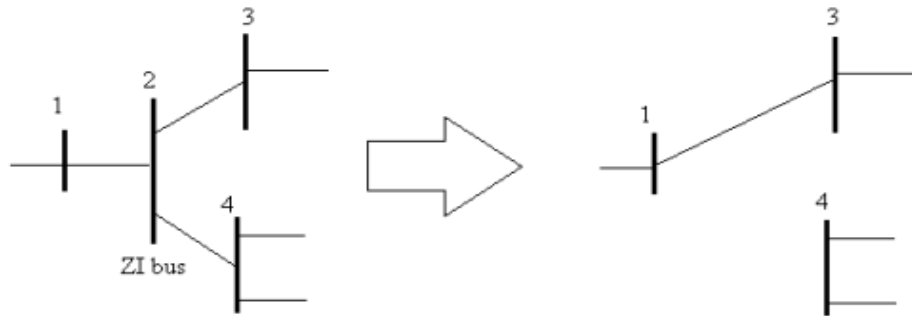


Figure 11- ZIB implementation rule number 3

- 4- When two or more ZIBs are linked together, these buses will be merged.

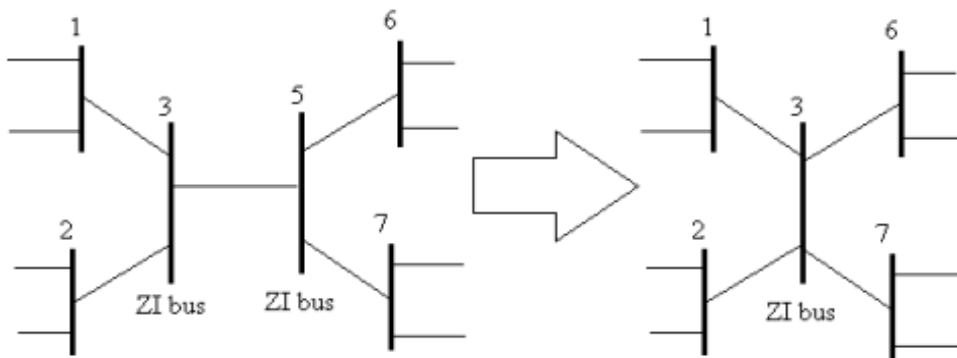


Figure 12- ZIB implementation rule number 4

- 5- Bus with minimum connections is eliminated if ZIB has more than three connections.

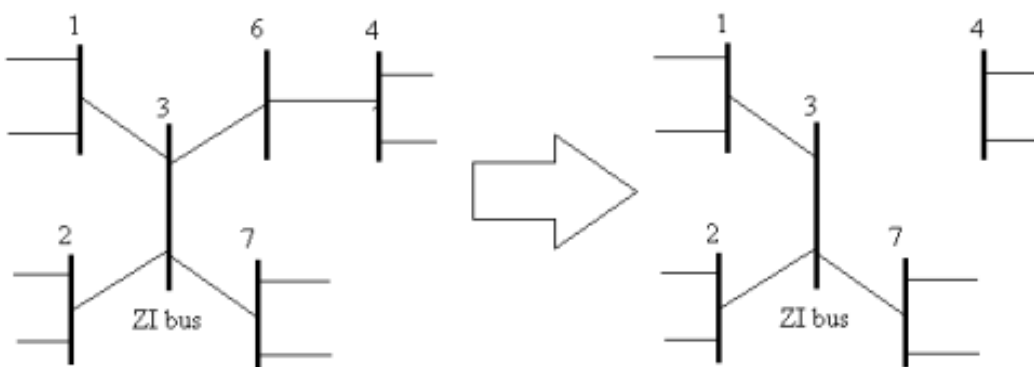


Figure 13- ZIB implementation rule number 5

Each PMU location is chosen individually using this algorithm. The following factor is used to determine the optimal placement of a PMU at each step:

$$Optimum_{Bus} = \max (\sum_{i=1}^N d_{ij} (\sum_{k=1}^N a_{ik})^{-2}) \quad j = 1, 2, 3, \dots, n \tag{3.1}$$

Where a^{ik} is an element in a modified connection matrix (A), and d_{ij} is the i^{th} row j^{th} column element in the connectivity matrix (D). The number of options for observing a given bus is shown by each row in the connectivity matrix. The quantity of connections for each bus is indicated in a column. The number of choices in a row is equal to the sum of the items in that row. A column's total number of connections is equal to the sum of its elements. To identify the new critical bus, every observable bus (its rows and columns) will be disregarded when the first PMU is installed. A new matrix (B) is found by the algorithm using (A and D).

At first, matrices A and D are equal (A = D). Matrix A is modified to disregard the observable buses for every iteration. Figure [14] shows the algorithm displayed as a matrix.

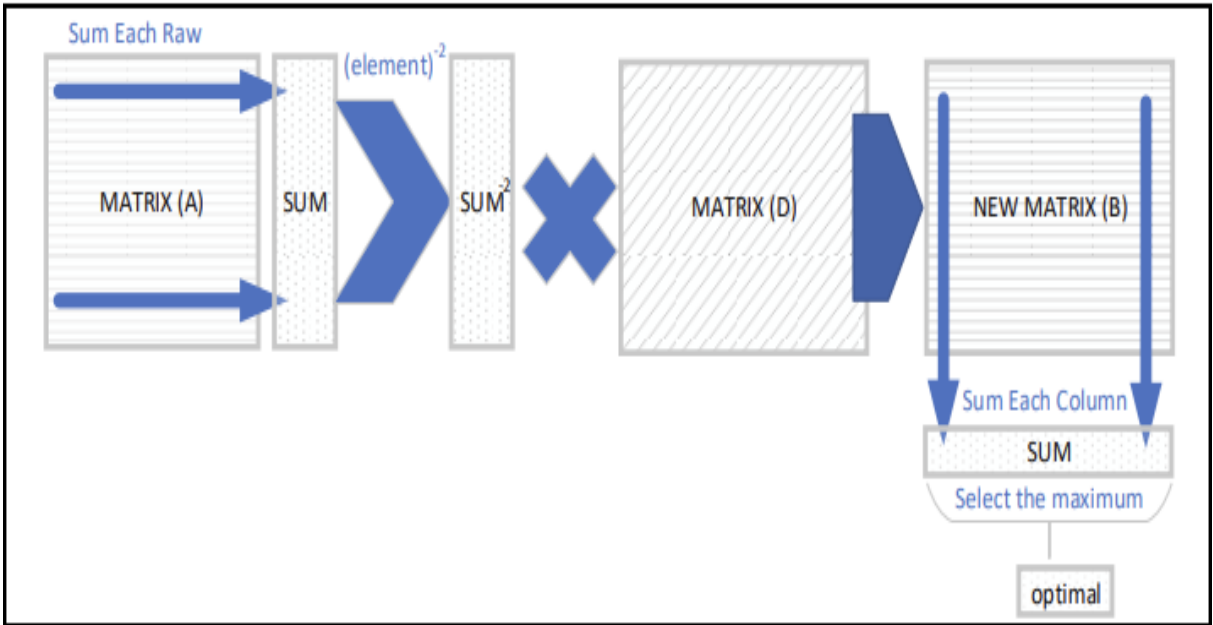


Figure 14- CMA's matrix format [29]

3.5 Testing for Validation

In this study, IEEE9-bus, 14-bus, 24-bus, 30-bus, 57-bus, and 118-bus test systems are used as transmission systems for validation testing. Table 1 illustrates the OPP findings based on the algorithm without taking ZIB into account, describing the optimal PMU locations required to attain total system observability. The table also shows the amount of computation time (in seconds) in each system, giving information about how effective the placement method is. The algorithm is validated with MATLAB R2024a.

Table 1 - Optimal PMU placement results without ZIB in different IEEE bus systems

SYSTEM	OPTIMAL PLACEMENT	NUMBER	TIME (S)
9- BUS	3, 4, 7	3	0.0272
14- BUS	2, 6, 7, 9	4	0.0209
24- BUS	2, 3, 8, 10, 16, 21, 23	7	0.0317
30- BUS	2, 3, 6, 10, 11, 12, 18, 23, 25, 29	10	0.0344
57- BUS	1, 6, 9, 15, 19, 21, 24, 25, 28, 32, 36, 38, 39, 41, 46, 50, 53	17	0.0379
118- BUS	3, 5, 9, 12, 13, 17, 21, 23, 25, 28, 34, 37, 41, 45, 49, 52, 56, 62, 64, 68, 71, 75, 77, 80, 85, 87, 90, 94, 101, 105, 110, 114	32	0.0557

Figures 15 and 16 present the IEEE 9-bus and IEEE 14-bus systems, respectively, serving as benchmarks for power system analysis without considering ZIBs. Phasor Measurement Units (PMUs) are represented by the blue circles in the figures, which show where they are located at particular buses.

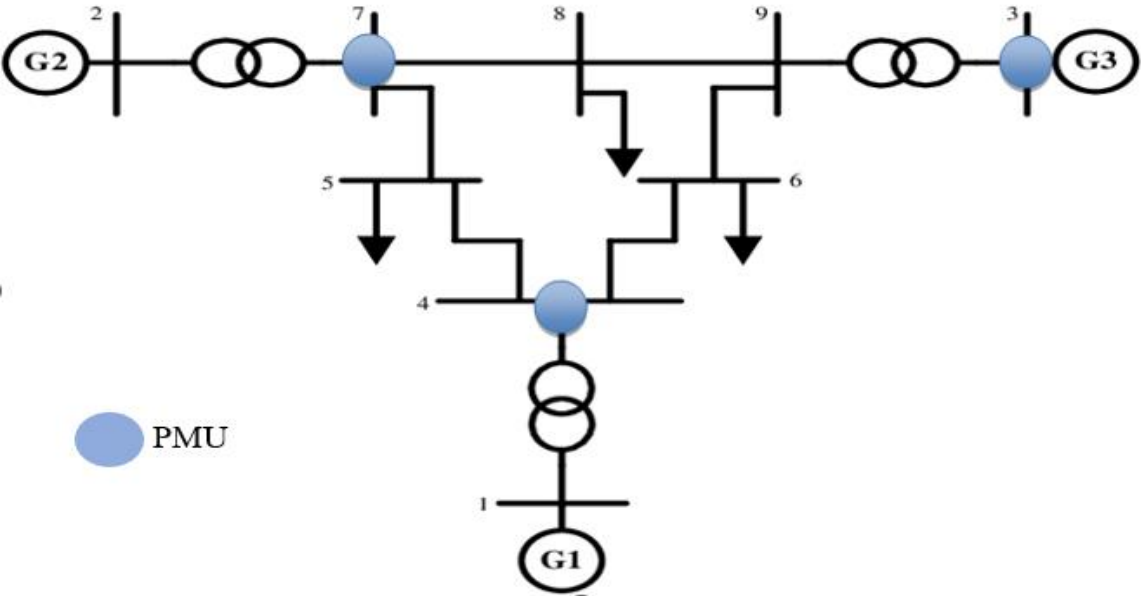


Figure 15- IEEE-9 bus system (without considering ZIB), 3 PMUs

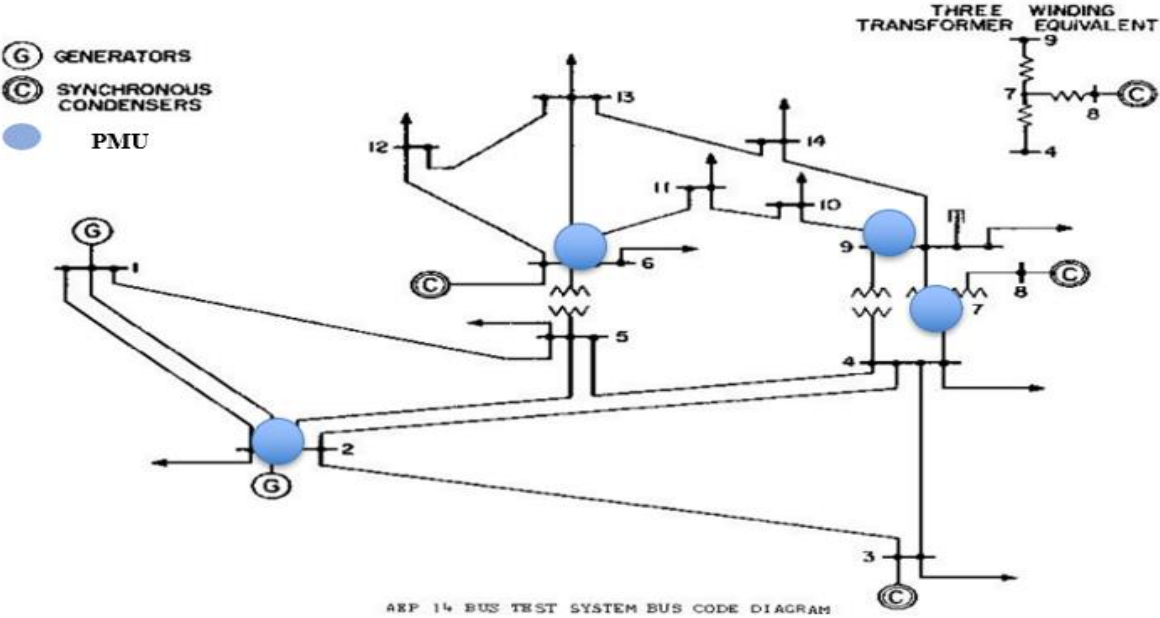


Figure 16- IEEE-14 bus system (without considering ZIB), 4 PMUs

In Table 2, the optimal PMU placement for different IEEE bus systems (with ZIB consideration) are compared. This inclusion is essential since it replicates more realistic conditions in which certain buses do not contribute to power generation or consumption. It

highlights the effect of ZIB on placement optimization by providing the number of PMUs needed for full network observability for systems ranging from 9-bus to 118-bus, together with the computational times attained.

Table 2 - Optimal PMU placement results with consideration of ZIB in different IEEE bus systems

SYSTEM	OPTIMAL PLACEMENT	NUMBER	TIME (S)
9- BUS	4, 7, 9	3	0.0258
14- BUS	2, 6, 9	3	0.0267
24- BUS	2, 8, 13, 15, 16, 20	6	0.0179
30- BUS	2, 3, 10, 12, 15, 19, 28	7	0.039
57- BUS	1, 4, 9, 15, 19, 25, 28, 32, 38, 43, 50, 53, 56	13	0.0245
118- BUS	3, 9, 11, 12, 17, 21, 27, 29, 32, 34, 38, 41, 45, 49, 52, 56, 62, 72, 75, 77, 80, 85, 87, 90, 94, 101, 105, 110	28	0.0482

Figures 17 and 18 depict the IEEE 9-bus and IEEE 14-bus systems, respectively, this time with incorporating ZIB. These diagrams illustrate the impact of ZIB on the bus system configurations, providing a more complex scenario for system stability analysis.

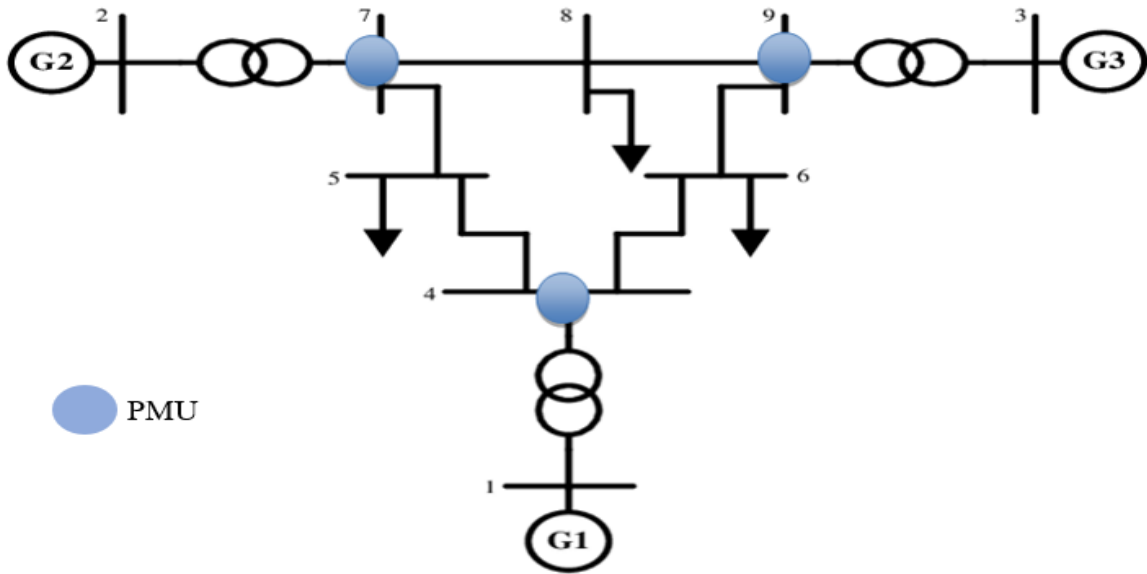


Figure 17- IEEE-9 bus system (with considering ZIB), 3 PMUs

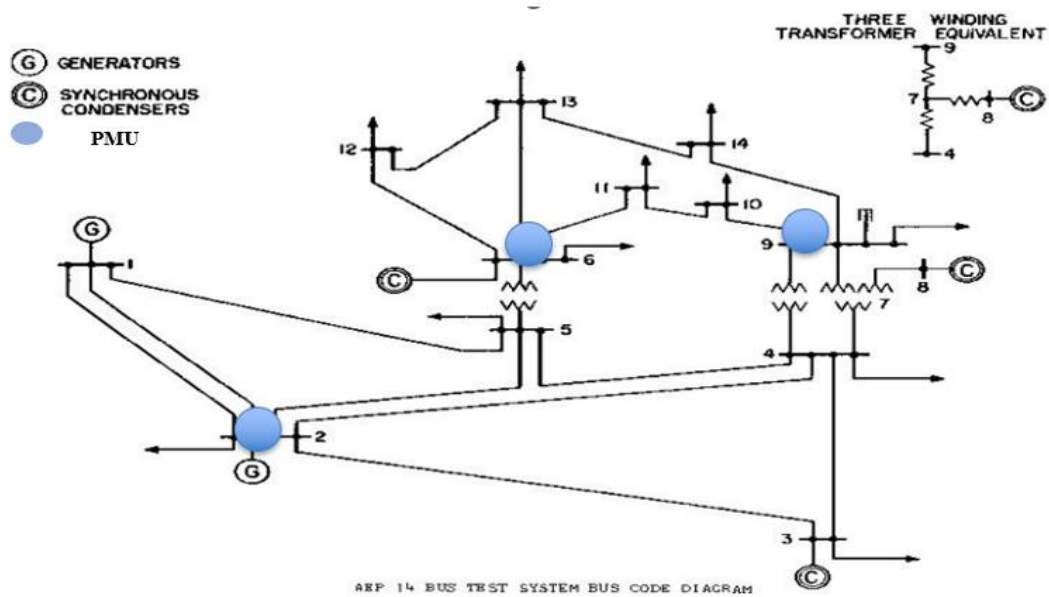


Figure 18- IEEE-14 bus system (with considering ZIB), 3 PMUs

According to the Table1 and Table2, short computation times demonstrated the efficiency of the technique in the computational analysis of PMU placement across different bus systems. Times ranged from 0.0272 seconds for the 9-Bus system to 0.0577 seconds for the 118-Bus system when Zero Injection Buses (ZIBs) were excluded. ZIB implementation has a negligible effect on these timings, somewhat raising them in smaller bus systems such as the 14-Bus system and decreasing them slightly in larger bus systems. These fast computation times

suggest that the algorithm has real-time power system monitoring potential. The analysis indicates that considering ZIBs in PMU placement reduces the number of PMUs required. ZIBs, which neither consume nor produce power, do not need direct monitoring. Their presence spreads observability throughout the grid without requiring PMUs on each bus, allowing the network's connectivity to be used more effectively.

To sum up, this chapter has explored the OPP problem in great detail and has shown how to achieve full observability in power systems using practical approaches. Through the use of algorithms like the CMA, it has been demonstrated how cost-effective strategic PMU placement may offer vital monitoring features. The outcomes highlight the algorithm's effectiveness, with calculation times appropriate for real-time applications, thereby confirming the potential of these approaches to improve power grid stability and reliability.

4. Wide Area Control (WAC) Strategy

4.1 Classification of Power System Stability

The quality of a power system that permits it to sustain a stable equilibrium while functioning normally or to return to an acceptable operational state following a little or major disturbance is known as power system stability. Power system instability is frequently caused by equipment losing synchronism, but it can also result from other factors such as abrupt voltage dips brought on by changes in load. Usually, the rotor and power angles between the machines show the stability. Minor disruptions such as regular load variations can occur, to which the system automatically adapts to maintain the appropriate voltage and frequency. Major disruptions, on the other hand, like transmission line problems or generator failures, drastically change the voltage and frequency of the system and set off control mechanisms to bring it back to normal. Power system stability is still a problem on a worldwide scale, and engineers' early efforts have made it possible for us to comprehend and address it today. Modeling disturbances and applying sophisticated simulations to precise stability studies are two ways to find solutions [39].

Power system stability has been categorized since it is impractical to examine system stability as it is. The concept and broad classification of the stability problem are shown in Figure 19.

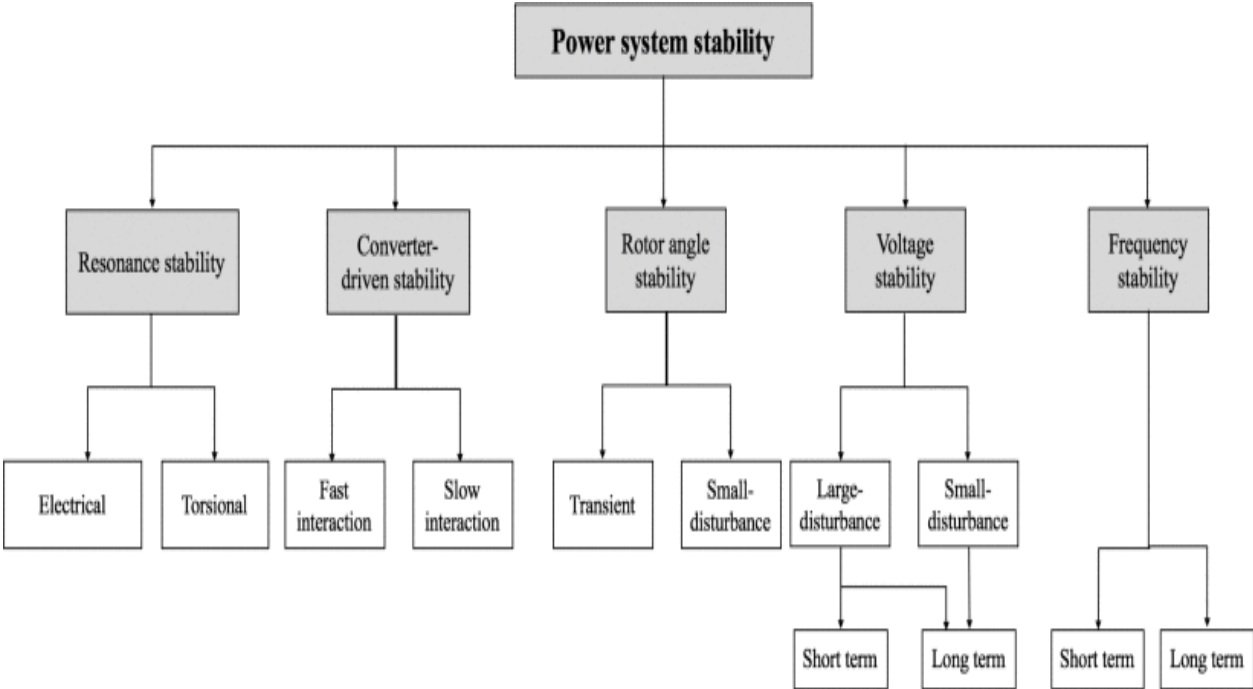


Figure 19 - Types of power system stability [40]

4.1.1 Rotor Angle Stability

Rotor angle stability guarantees that, in the event of a disturbance, synchronous machines in a power system stay in sync. In order to understand power output variations brought on by rotor angle oscillations, it is necessary to analyze how one machine's rotor angle varies in relation to the others. Variations in power input have an impact on power output because they alter the rotor angle, which is the angle formed by the stator's revolving magnetic field and rotating shaft. Machines accelerate or decelerate in response to disturbances, which modifies the distribution of the load and brings the system to a new equilibrium. On the other hand, synchronism may be lost as a result of large speed variations. Small signal stability and transient stability are two categories for rotor angle stability. This thesis primarily focuses on issues related to small signal stability.

4.1.2 Small Signal Stability

Small signal stability is the capacity of a system to maintain synchronization in the face of small disturbances, such as variations in load and generation. Because of how small these disturbances are, power system studies can use a linear system model and use eigenvalue analysis. Two types of small signal stability exist: global and local stability. While global stability deals with inter-area oscillations—the interaction of generator groups in different areas—local stability deals with a single generator's reaction to small system changes. Due to the fact that, inter-area oscillations are more complicated, they must be carefully dampened to avoid getting worse. Effective tools for reducing these oscillations include compensators, Automatic Voltage Regulators (AVRs), and Power System Stabilizers (PSSs) [41].

In this thesis, the main focus is on damping these low frequency oscillations in wide area of power system using PSDAT/ MATLAB package toolbox.

4.2 Power System Dynamic Analysis Toolbox (PSDAT)

There are some methods which they used to study the dynamic behavior of an interconnected power system including: frequency response analysis, modal analysis, and time-domain simulation. A system of Differential Algebraic Equations (DAEs) can be used to mathematically model a multi-machine power system in the time domain. There are two ways to solve these equations: explicitly and implicitly. Using a numerical technique like Euler's or the trapezoidal method, the Differential Equations (DEs) are transformed into Algebraic

Equations (AEs) in the implicit method. The new equations are algebraic in nature and can be solved numerically in parallel. In the explicit technique, AEs are solved separately for algebraic variables and DEs are solved independently for state variables using numerical integration. Other analysis types include frequency response and modal analyses for small-signal investigations, which need linearizing the nonlinear equations of the power system around an operational point in order to describe the system in state-space. PSDAT which stands for Power System Dynamic Analysis Toolbox developed by Ismael Abdulrahman [33] is a package of MATLAB-based and also Simulink-based program. It is a useful tool for academic studies and educational purposes. The PSDAT models don't have any for-loops and instead of that the system is vectorized, with vectors and matrices serving as the foundation for the DAEs structure that represents the system.

4.2.1 PSDAT Capabilities

PSDAT can simulate large-scale power systems with thousands of buses, in contrast to Power System Analysis Toolbox (PSAT), which is best suited for smaller systems. PSAT necessitates individual component representation, which means that many generator and bus blocks, loads, and transmission lines must be included in order to replicate a particular test system. In contrast, PSDAT employs, independent of system size, a uniform block diagram structure (in Simulink) or coded DAEs in MATLAB. Because every block and signal in Simulink is vectorized, simulating various systems is made easier by simply requiring changes to fixed parameters—such as the admittance matrix, which is already computed in MATLAB. As a result, PSDAT offers comprehensive simulation capabilities for power systems in MATLAB and Simulink, covering time-domain, modal, and frequency response analyses [33].

In order to fully comprehend generator behavior in power systems, a comprehensive list of electrical, mechanical, and control-related characteristics and variables is included in table 3. These parameters and variables are utilized in the analysis of the dynamics and control of synchronous generators.

Table 3- Parameters and variables for synchronous generator dynamics and control [33]

R_s : Stator resistance (pu)	I_{Gi} : Current magnitude of generator (pu)
X_d : d-axis reactance (pu)	γ_i : Angle of generator current (rad)
X'_d : d-axis transient reactance (pu)	I_d : d-axis current (pu)
X''_d : d-axis sub-transient reactance (pu)	I_q : q-axis current (pu)
X_q : q-axis reactance (pu)	α_{iK} : Admittance angle Y_{iK} (rad)
X'_q : q-axis transient reactance (pu)	E_{fd} : Field voltage (pu)
X''_q : q-axis sub-transient reactance (pu)	V_R : Exciter input (pu)
H : Shaft inertia constant (s)	R_F : Feedback rate (pu)
ω_s : Synchronous speed of the generator (rad/s)	T_M : Torque applied mechanically (pu)
T'_{do} : The time constant d-axis related to E'_q (s)	P_{SV} : Steam valve position (pu)
T''_{do} : The time constant d-axis related to Ψ_{1d} (s)	P_C : Control power input (pu)
T'_{qo} : The time constant q-axis related to E'_d (s)	R_D : Quantity of speed regulation (Hz/pu)
T''_{qo} : The time constant q-axis related to Ψ_{2q} (s)	V_{ref} : Reference voltage input (pu)
T_A : Time constant of the amplifier (s)	S_E : Saturation function
T_{CH} : Steam chest time constant incrementally (s)	T_{FW} : Torques of frictional windage
T_{SV} : Duration of steam valve (s)	δ : Angle of rotor (rad)
K_A : Gain of Amplifier	ω : Generator's angular velocity (rad/s)
K_{AE} : Independent or self-stimulating constant	\bar{V}_i : Complex voltage phasor
E'_q : Transient internal voltages of q-axis (pu)	V : Bus voltage magnitude (pu)
E'_d : Transient internal voltages of d-axis (pu)	θ : Bus voltage angle (rad)
E : Internal voltage (pu)	\bar{I}_{Gi} : Generator complex current phasor
Ψ_{1d} : Damper winding 1d flux-linkages (pu)	
Ψ_{2q} : Damper winding 2q flux-linkages (pu)	

4.3 System Modeling

The Differential Algebraic Equations (DAEs) of a multi-machine power system with m machines and n buses can be written as follows [34]:

4.3.1 Synchronous Generator

$$T'_{doi} \frac{dE'_{qi}}{dt} = -E'_{qi} - (X_{di} - X'_{di}) \left[I_{di} - \frac{(X'_{di} - X''_{di})}{(X'_{di} - X_{ls})^2} (\Psi_{1di} + (X'_{di} - X_{ls})I_{di} - E'_{qi}) \right] + E_{fd} \quad (4.1)$$

$$T''_{doi} \frac{d\Psi_{1di}}{dt} = -\Psi_{1di} + E'_{qi} - (X'_{di} - X_{ls})I_{di} \quad (4.2)$$

$$T'_{qoi} \frac{dE'_{di}}{dt} = -E'_{di} - (X_{qi} - X'_{qi}) \left[I_{qi} - \frac{(X'_{qi} - X''_{qi})}{(X'_{qi} - X_{ls})^2} (\Psi_{2qi} + (X'_{qi} - X_{ls})I_{qi} - E'_{di}) \right] \quad (4.3)$$

$$T''_{qoi} \frac{d\Psi_{2qi}}{dt} = -\Psi_{2qi} + E'_{di} - (X'_{qi} - X_{ls})I_{qi} \quad (4.4)$$

$$\frac{d\delta_i}{dt} = \omega_i - \omega_s \quad (4.5)$$

$$\frac{2H_i}{\omega_s} \frac{d\omega_i}{dt} = T_{Mi} - \frac{(X''_{di} - X_{ls})}{(X'_{di} - X_{ls})} E'_{qi} I_{qi} - \frac{(X'_{di} - X''_{di})}{(X'_{di} - X_{ls})} \Psi_{1di} I_{qi} - \frac{(X''_{qi} - X_{ls})}{(X'_{qi} - X_{ls})} E'_{di} I_{di} + \frac{(X'_{qi} - X''_{qi})}{(X'_{qi} - X_{ls})} \Psi_{2qi} I_{di} - (X''_{qi} - X''_{di}) I_{di} I_{qi} - T_{FW} \quad (4.6)$$

4.3.2 Excitation System

$$T_{Ei} \frac{dE_{fdi}}{dt} = - (K_{Ei} + S_{Ei}(E_{fdi})) E_{fdi} + V_{Ri} \quad (4.7)$$

$$T_{Fi} \frac{dR_{fi}}{dt} = -R_{fi} + \frac{K_{fi}}{T_{fi}} E_{fdi} \quad (4.8)$$

$$T_{Ai} \frac{dV_{Ri}}{dt} = -V_{Ri} + K_{Ai} R_{fi} - \frac{K_{Ai} K_{fi}}{T_{fi}} E_{fdi} + K_{Ai} (V_{refi} - V_i) \quad (4.9)$$

4.3.3 Turbine System

$$T_{Chi} \frac{dT_{Mi}}{dt} = -T_{Mi} + P_{Svi} \quad (4.10)$$

$$T_{Svi} \frac{dP_{Svi}}{dt} = -P_{Svi} + P_{Ci} - \frac{1}{R_{Di}} \left(\frac{\omega_i}{\omega_s} - 1 \right) \quad (4.11)$$

4.3.4 Algebraic Equations (Stator and Power Flow)

$$0 = R_{si} I_{di} - X''_{qi} I_{qi} - \frac{(X''_{qi} - X_{ls})}{(X'_{qi} - X_{ls})} E'_{di} + \frac{(X'_{qi} - X''_{qi})}{(X'_{qi} - X_{ls})} \Psi_{2qi} + V_i \sin(\delta_i - \theta_i) \quad (4.12)$$

$$0 = R_{si} I_{qi} + X''_{di} I_{di} - \frac{(X''_{di} - X_{ls})}{(X'_{di} - X_{ls})} E'_{qi} - \frac{(X'_{di} - X''_{di})}{(X'_{di} - X_{ls})} \Psi_{1di} + V_i \cos(\delta_i - \theta_i) \quad (4.13)$$

$$I_{di} V_i \sin(\delta_i - \theta_i) + I_{qi} V_i \cos(\delta_i - \theta_i) + P_{Li}(V_i) - \sum_{k=1}^n V_i V_k Y_{ik} \cos(\theta_i - \theta_k - \alpha_{ik}) = 0 \quad (4.14)$$

$$I_{di} V_i \cos(\delta_i - \theta_i) - I_{qi} V_i \sin(\delta_i - \theta_i) + Q_{Li}(V_i) - \sum_{k=1}^n V_i V_k Y_{ik} \sin(\theta_i - \theta_k - \alpha_{ik}) = 0 \quad (4.15)$$

$$P_{Li}(V_i) - \sum_{k=1}^n V_i V_k Y_{ik} \cos(\theta_i - \theta_k - \alpha_{ik}) = 0 \quad (4.16)$$

$$Q_{Li}(V_i) - \sum_{k=1}^n V_i V_k Y_{ik} \sin(\theta_i - \theta_k - \alpha_{ik}) = 0 \quad (4.17)$$

where for all state variables, machine inputs, and references, $i = 1, 2, \dots, m$. For the load flow analysis, the ik^{th} entries of the admittance matrix are utilized. $V_i, \theta_i, I_{di}, I_{qi}$ are found by solving $(n + m)$ complex AEs for a given load power. Additionally, there should be a maximum and minimum value for the V_R and P_{SV} outputs.

4.3.5 Load Model

Loads consist of an equal amount of constant impedance, constant current, and constant power. The loads are represented by the equation below [35].

$$P_{Li} = P_{L0} \left(\frac{V_i}{V_0}\right)^\alpha \quad Q_{Li} = Q_{L0} \left(\frac{V_i}{V_0}\right)^\beta \quad (4.18)$$

where α and β are the active and reactive load parameters, respectively, and P_{Li}, Q_{Li} and V_i are the steady-state values of active power, reactive power, and voltage magnitude acquired from load flow analysis prior to a disturbance. When the loads are treated as constant power (voltage-independent), constant current (voltage-dependent), and constant voltage (voltage-dependent), respectively, these parameters may have a value of 0, 1, or 2.

4.3.6 Reference Angle

There should be a reference for the rotating components of a dynamic system. The angle variables' plots continuously rise in the absence of a reference. One widely-used tool is the Center of Inertia (COI), which is described as follows [34].

$$\delta_{COI} = \frac{\sum_1^m M_i \delta_i}{\sum_1^m M_i}, \quad \omega_{COI} = \frac{\sum_1^m M_i \omega_i}{\sum_1^m M_i} \quad (4.19)$$

Where $M_i = \frac{2 \cdot H_i}{\omega_i}$. Since the angle variables in equations (4.12) through (4.17) are always difference pairs, adding a reference for the angles is unnecessary because they cancel out each other. To achieve an acceptable transformation, substitute the rotating signal ω_{COI} for the constant ω_s in equation (4.5). In this study, the rotating components of the system are referenced by ω_{COI} .

4.3.7 Initial Conditions Calculation

Finding the initial values for state variables and constant inputs, as well as the steady-state values for algebraic variables, is the first step in solving a dynamic system. Calculating bus voltage phasors $\bar{V}_i = V_i e^{j\theta_i}$ is one aspect of this as well as generator output powers ($P_{Gi} + Q_{Gi}$). MATPOWER is an open-source package in MATLAB that includes tools for regular and optimal power flow and can be used for load flow analysis. To obtain the initial conditions for the state variables, put the derivative terms of the differential-algebraic equations to zero [36]. The process in which the initial values were computed is available in [33]. Several analytical control tools are used to analyze the behavior of systems, especially in dynamics. Time domain analysis, pole-zero plots, modal analysis, frequency response analysis, and participation factor mapping are some of these methods. To understand the dynamic properties of the system, this study has used pole-zero plots, modal analysis, and frequency response analysis.

4.4 Modal Analysis [37]

A set of linear DAEs is obtained by linearizing the nonlinear DAEs around the operational point $\{x_0, y_0, z_0\}$:

$$\begin{aligned}\dot{x} &= f(x, z, u) \\ 0 &= g(x, z, u) \\ y &= h(x, z, u)\end{aligned}\tag{4.20}$$

where x , z , u , and y represent the vectors of state variables, algebraic variables, inputs, and outputs, respectively, and f , g , and h represent the vectors of differential equations, algebraic equations, and output equations.

The set of equations that result from linearizing (4.20) around an operating point $\{x_0, y_0, z_0\}$ is as follows:

$$\begin{aligned}\Delta\dot{x} &= \frac{\partial f}{\partial x} \Delta x + \frac{\partial f}{\partial z} \Delta z + \frac{\partial f}{\partial u} \Delta u \\ 0 &= \frac{\partial g}{\partial x} \Delta x + \frac{\partial g}{\partial z} \Delta z + \frac{\partial g}{\partial u} \Delta u \\ \Delta y &= \frac{\partial h}{\partial x} \Delta x + \frac{\partial h}{\partial z} \Delta z + \frac{\partial h}{\partial u} \Delta u\end{aligned}\tag{4.21}$$

The linearized DAEs can be expressed in the following state-space form by removing the algebraic variable vector:

$$\begin{aligned}\Delta\dot{x} &= A \Delta x + B \Delta u \\ \Delta y &= C \Delta x + D \Delta u\end{aligned}\tag{4.22}$$

where the partial derivative matrices of the original system, as given in (4.20) can be expressed in the following form: A (state matrix), B (input matrix), C (output matrix), and D (feed-forward matrix):

$$\begin{aligned}A &= \left[\frac{\partial f}{\partial x} - \frac{\partial f}{\partial z} \left(\frac{\partial g}{\partial z} \right)^{-1} \frac{\partial g}{\partial x} \right] \\ B &= \left[\frac{\partial f}{\partial u} - \frac{\partial f}{\partial z} \left(\frac{\partial g}{\partial z} \right)^{-1} \frac{\partial g}{\partial u} \right] \\ C &= \left[\frac{\partial h}{\partial x} - \frac{\partial h}{\partial z} \left(\frac{\partial g}{\partial z} \right)^{-1} \frac{\partial g}{\partial x} \right] \\ D &= \left[\frac{\partial h}{\partial u} - \frac{\partial h}{\partial z} \left(\frac{\partial g}{\partial z} \right)^{-1} \frac{\partial g}{\partial u} \right]\end{aligned}\tag{4.23}$$

4.4.1 Eigenvalue, Eigenvector, Damping Ratio, and Frequency

The matrices A , B , C , and D are computed after the system in Simulink is linearized around an operational point. The eigenvalues of the system ($\lambda = \sigma \pm \omega$) and the right-left eigenvectors from these matrices are found using the MATLAB software, where σ is the real part of the eigenvalue (λ) and ω is the imaginary portion of λ . Then, using the formulas $(\frac{\omega}{2\pi})$ and $(\frac{-\sigma}{\sqrt{\sigma^2 + \omega^2}} * 100\%)$, respectively, the frequency in Hz and damping ratio in % for each oscillatory mode are calculated.

4.4.2 Mode Shape

The relative activity between the modes and the state variables can be calculated using the mode shape. It offers crucial details regarding the role that state variables play in the excitation of critical modes. The polar plot of the linearized system's right eigenvector matrix is the mathematical representation of the mode shape. Designing control solutions that improve system stability and comprehending resonance events require a thorough analysis of the mode shape.

4.5 Frequency Response Analysis [37]

Apart from modal analysis, frequency response analysis is another key method for examining the dynamic behavior of power systems, utilizing Bode, Nyquist, and Nichols diagrams. For a closed-loop system to be stable, the open-loop gain and phase margins derived from the Bode diagram should be positive and sufficiently large. Typical design values for gain and phase margins are around 6 dB and 30° to 60°, with an average of about 45°, respectively. The Nyquist and Nichols diagrams also provide insight into the system's stability. In these approaches, the critical point is $(-1, 0)$ on the Nyquist plot. The critical point must be far from the Nichols plot, while the Nyquist plot of the open-loop transfer function must not encircle it in order for a closed-loop to be stable.

4.6 Simulation Results (Without controller)

This part uses the IEEE 9-bus network as a test system. The generator and excitation system's dynamic data, transmission lines, and power flow data are all located in [34]. For the IEEE 9-bus, the machine sub-transient and turbine parameters are computed in [38].

To assess the stability of the systems, three scenarios have been conducted without presence of controller using PSDAT package. including:

- Tie-Line Scenario
- Bus Data Scenario
- Power Systems Integrated with a Renewable Energy Resource (RES) Scenario

4.6.1 Tie-line Scenario Analysis

The MATPOWER simulation results for an IEEE-9 bus system with several area configurations are shown in Table 4.

Table 4 – Tie-lines analysis with total inter-tie flows and convergence time in various IEEE-9 bus configurations

SYSTEM	AREAS & BUSES	P(MW)	Q(MVAR)	CONVERGENCE TIME (S)
ONE AREA	-	0	0	0.06
TWO AREAS	Area 1: 1,4,5,6 Area 2: 2,3,7,8,9	145.6	3.8	0.07
THREE AREAS	Area 1: 1,4,5 Area 2: 2,7,8 Area 3: 3,6,9	140.2	24	0.08

A single-area system demonstrated a quick 0.06-second convergence time and no inter-area flows. The inter-area power flow was 145.6 MW and 3.8 MVAR with a convergence time of 0.07 seconds when the system was split into two areas (buses 1, 4, 5, 6 in Area 1 and buses 2, 3, 7, 8, 9 in Area 2). The division of the system into three areas (Area 1: buses 1, 4, 5;

Area 2: buses 2, 7, 8; Area 3: buses 3, 6, 9) produced a convergence time of 0.08 seconds, an increase in reactive power exchange of 24 MVAR, and a somewhat reduced active power flow of 140.2 MW. The Newton's approach converged in four rounds across configurations, indicating stable computing in spite of the system's increased subdivision. As a result, The IEEE 9-bus system's overall stability is unaffected by dividing into different areas, although it does cause a modest increase in convergence time and complexity in reactive power management. The inter-area power flows in the simulations are stable, with a slight drop in power transferred as the number of areas increases.

The modes with insufficient damping are depicted in Figure 20 using PSDAT package for all above-mentioned IEEE-9 bus configurations (One-Area, Two-Area, Three-Area). As illustrated, $-1.014 \pm 14.9i$ and $-0.53 \pm 8.93i$ are the two lightly-damped modes for this system. These two modes have respectively frequencies of 2.37 Hz and 1.422 Hz and damping ratios of 6.81% and 5.98%. When it comes to the modes, the phase angle offers the phase displacement, while the mode shape's magnitude indicates the level of contribution from the state variables in the modes. As can be seen in Figure 20 (left), there is a 180-degree phase difference between the rotor speed deviations of Generator1 and Generators2-3, indicating that Generator1 swings against Generators2-3. Generator3 swings in opposition to the other two generators for the second, lightly-damped mode depicted in Figure 20 (right).

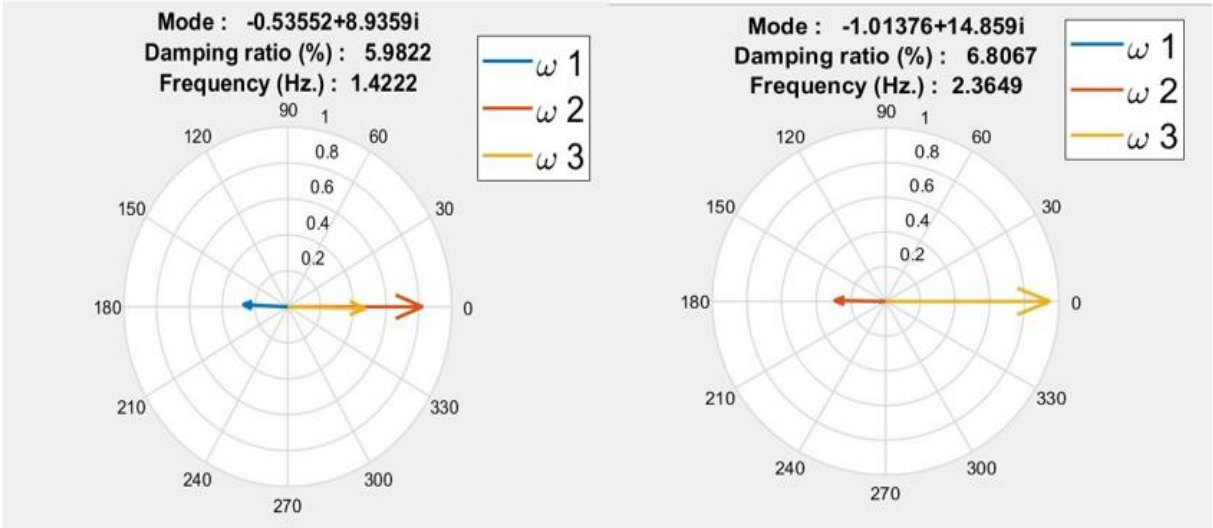


Figure20- Visualizations of the mode shape for rotor speed state variables and lightly damped modes of IEEE-9 bus systems (One-area, Two-area, Three-area)

Figure 21 displays the frequency response analysis of the systems (One-Area, Two-Area, Three-Area) using PSDAT package, along with Bode and Nichols diagrams. The closed-loop

transfer function for the Bode diagram (right) is stable because the phase and gain margins are both positive and sufficiently large. The plot of the Nichols diagram (left) does not cross or get close to the crucial point (180°,0). Moreover, the pole-zero map depicted in Figure 22 represents all systems (One-area, Two-area, Three-area), with all poles located on the left-hand side of the plane. This placement indicates that each system is stable, as poles in the left-half plane are a criterion for system stability

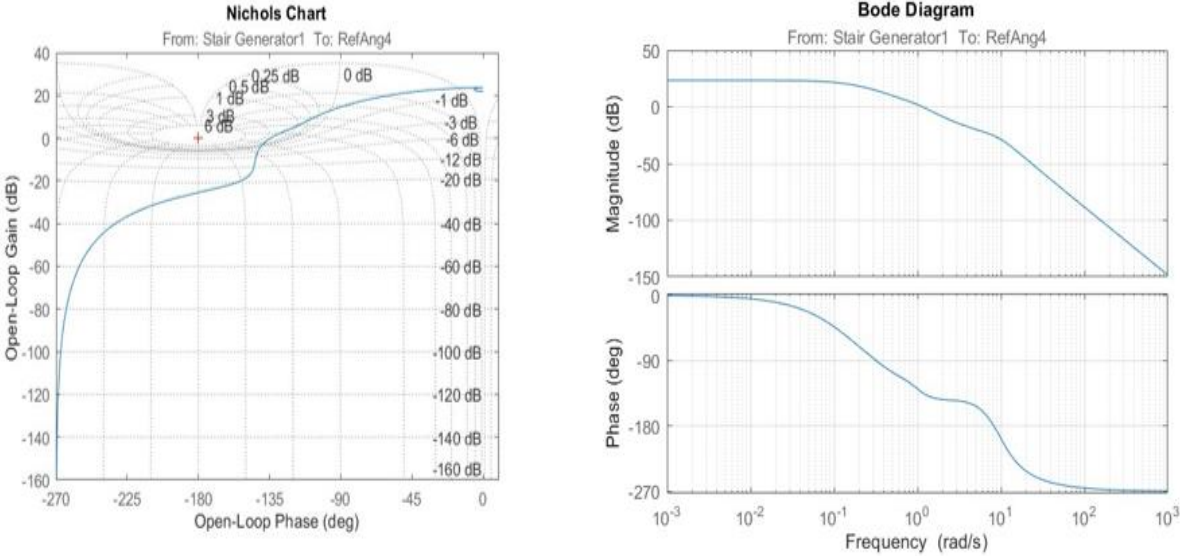


Figure 21- Frequency response analysis: Nichols's plot (left) and Bode plot (right) Of all systems (One-area, Two-area, Three-area)

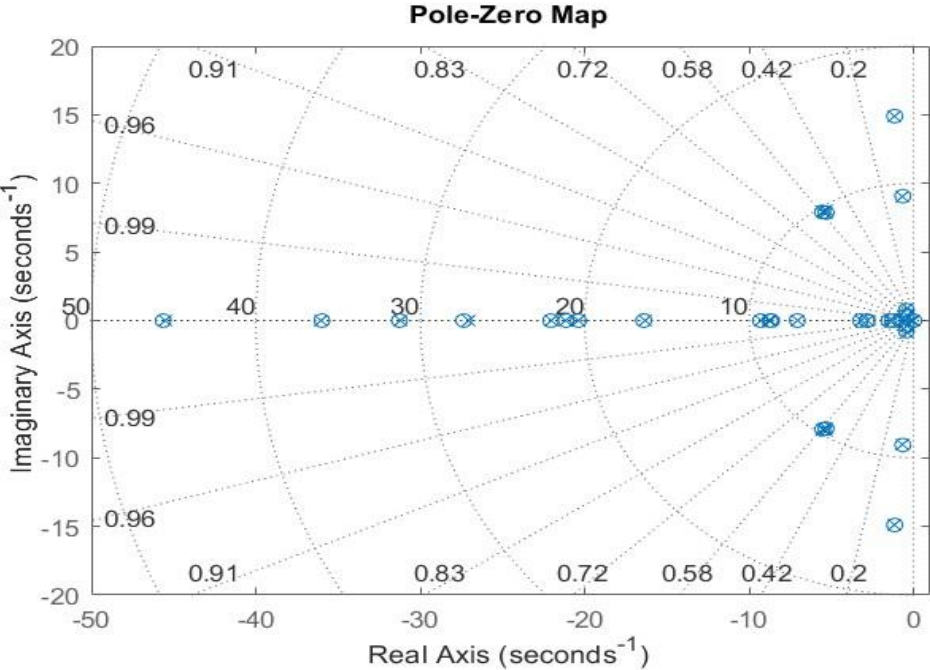


Figure 22- Pole-zero map of all the systems (One-area, Two-area, Three-area)

4.6.2 Branch Data Scenario Analysis

As can be seen in Figure 23, the two-area IEEE-9 bus 3-machine dynamic test system, operating without a controller, is analyzed using modal analysis and pole-zero mapping to get insights into stability issues. The presence of undamped inter-area oscillations is indicated by the modal analysis using PSDAT, highlighting system instability. This section specifically focusing on the effects of line impedance modifications on system stability. By increasing the line impedances in lines 4-6, 6-9 and 3-9 it was observed that the system became unstable.

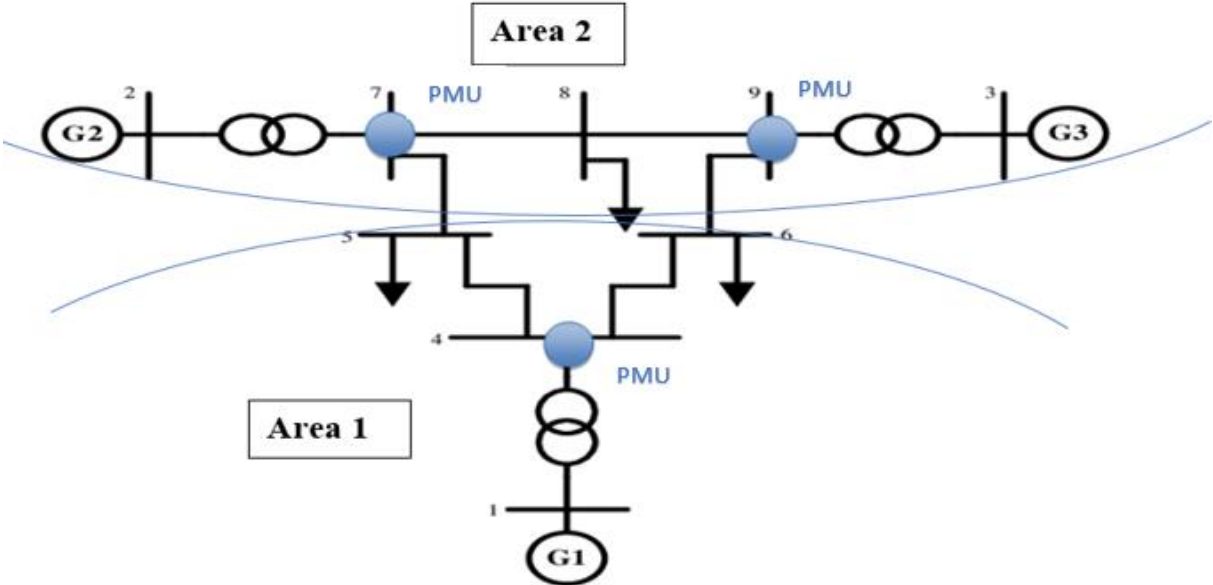


Figure 23- Two area IEEE-9 bus test system

The simulation results, presented in Figure 24, identify modes with low damping ratios. Notably, a mode with a negative damping ratio, which indicative of system instability, is observed at a frequency of 0.11649 Hz, and falls within the typical inter-area oscillation range of 0.1 to 0.8 Hz [26]. This mode, involving all rotating components across the tie-line, is identified as a primary source of instability and inter-area oscillations. Moreover, as illustrated in Figure 25 the pole-zero map of the system showed an unstable mode with a positive real component of the eigenvalue ($0.421 + 0.731i$), further confirming the instability introduced by the line impedance modifications.

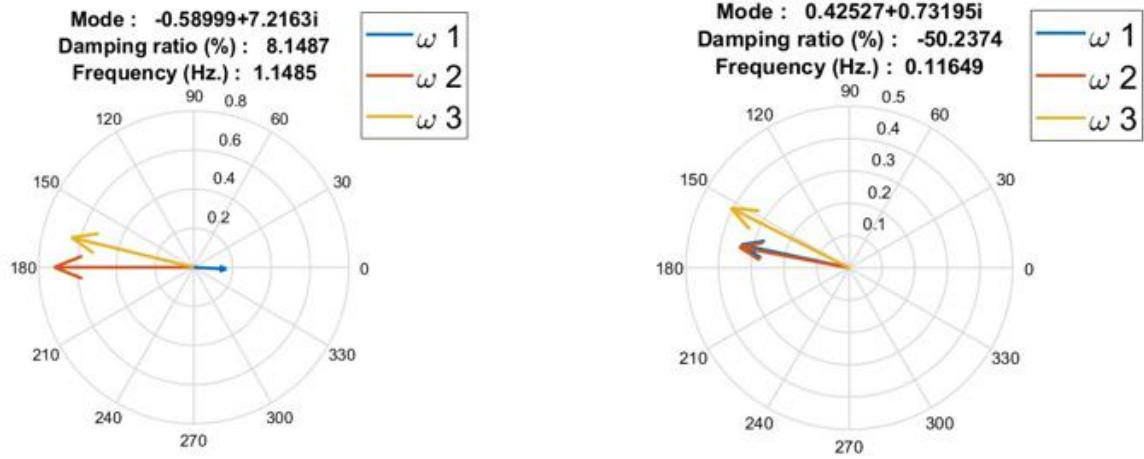


Figure 24- Mode shapes plots without controller

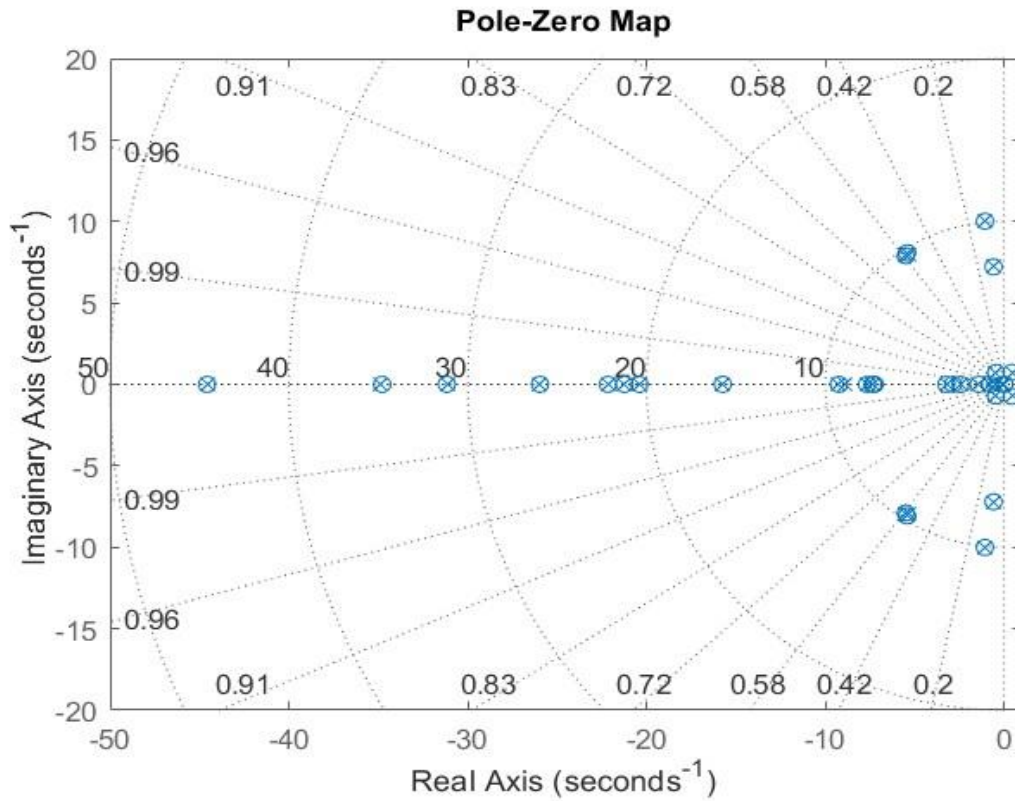


Figure 25- Pole-zero map of the system without controller

4.6.3 Power System Integrated with a Renewable Energy Source (RES) Scenario Analysis

To investigate the impact of integrating a Renewable Energy Source (RES) into the IEEE-9 bus 3-machine two-area test system, a conventional generator, G1, was replaced with a renewable generator model, as illustrated in Figure 26. This replacement aims to study the dynamics and stability of the power system when traditional generation sources are substituted with renewable technologies like wind turbines, solar panels, or energy storage systems using the generic model which is explained in more detail in [42]. Modal analysis and pole-zero mapping were conducted to assess the system's response to this integration.

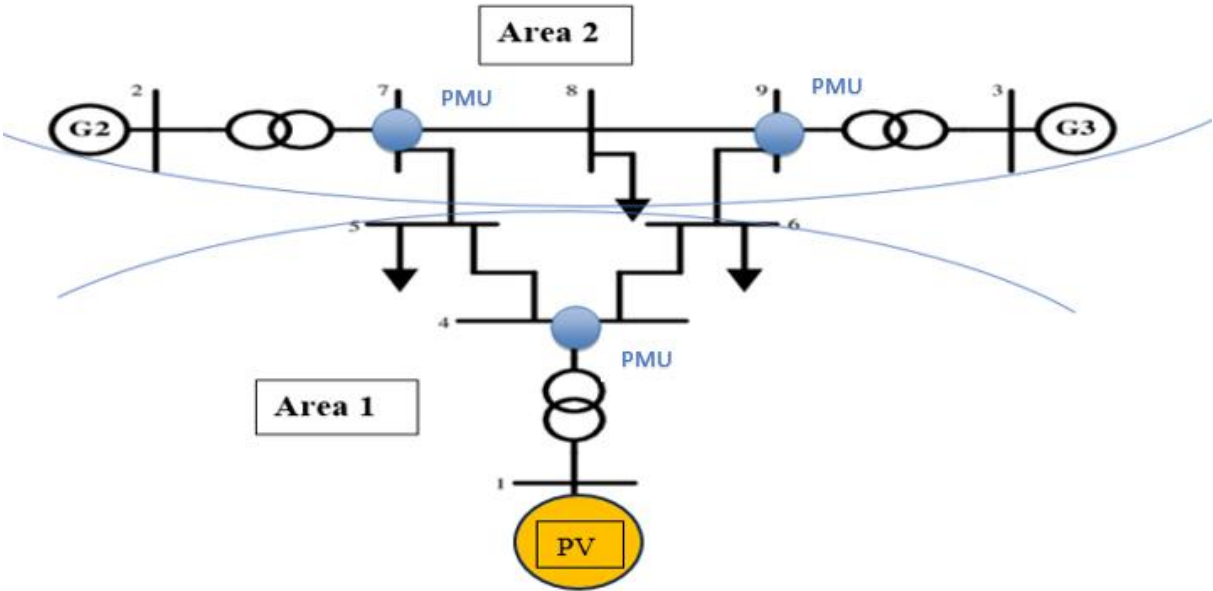


Figure 26- Two area IEEE-9 bus test system (with G1 replaced by a PV plant)

The findings which are demonstrated in Figure 27 reveal a critical mode with a negative damping ratio, indicating potential instability, yet the mode's frequency of 0.03 Hz categorizes it outside the typical inter-area oscillation range of 0.1 to 0.8 Hz. This suggests that while the system may exhibit signs of instability, it does not engage in the typical inter-area oscillations that are often critical in larger grid interactions. According to [43] in addition to the inter-area oscillations, the system may also exhibit a phenomenon referred to as common low-frequency oscillations, typically ranging from 0.01 to 0.1 Hz. This type of oscillation can arise within interconnected systems due to incorrect speed governor control of the power system's hydro or thermal units.

Additionally, the pole-zero map in Figure 28 shows an unstable mode with a positive real component of its eigenvalue ($0.53 + 0.186i$), highlighting the complexities and challenges associated with integrating renewable energy sources into existing grid infrastructure without robust control strategies.

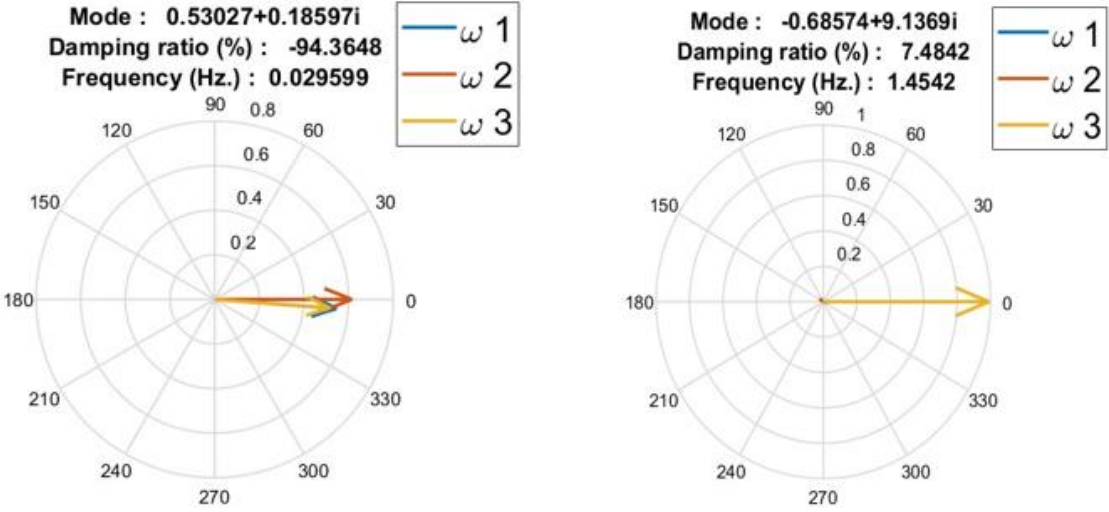


Figure 27- Mode shapes plots without controller (with G1 replaced by a PV plant)

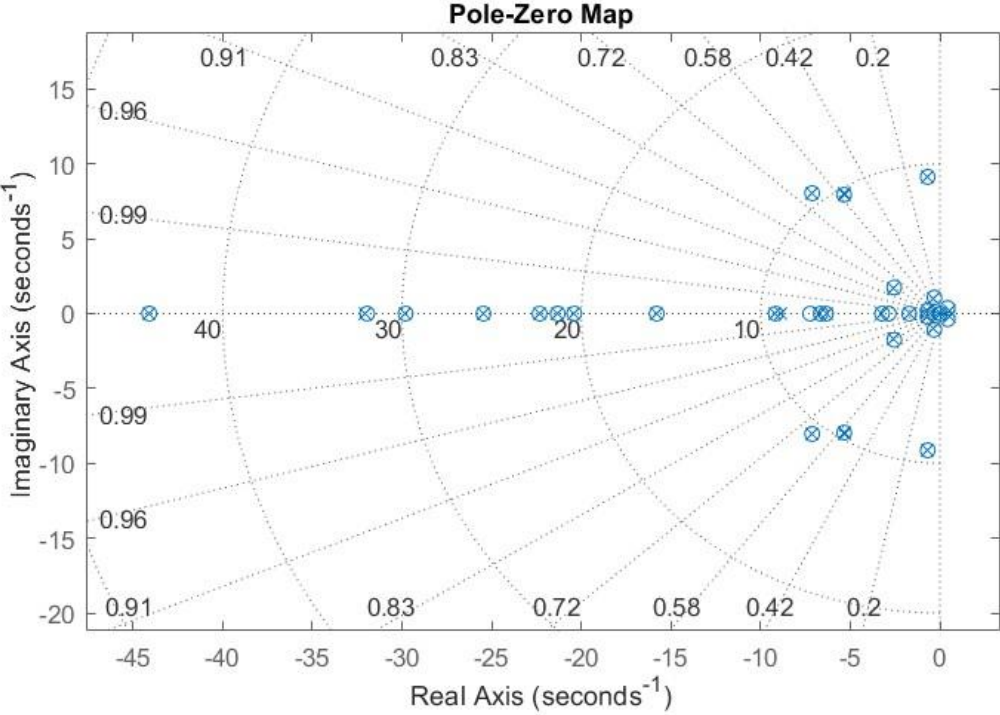


Figure 28- Pole-zero map of the system without controller (with G1 replaced by a PV plant)

4.7 Model-Based & Model-Free Control in Power Systems

Model-based and model-free control strategies are used in power systems. Controllers in model-based systems are represented by mathematical formulas. It might be difficult to create detailed physical models for interconnected systems with big state and action spaces when designing model-based controllers for complex systems with uncertainties. Conversely, model-free controllers depend on learning and mapping of input-output data. Since they base their decisions on measurements from the internet, they do not require internal model knowledge or equations. Because of this, model-free controllers can be used to solve control problems in complex large-scale power systems. Smart grids with sophisticated sensors give huge data that intelligent agents can use to maximize control. The cutting edge of model-free controller technology is Machine Learning (ML). Reinforcement Learning (RL) for dynamic environments, supervised learning for clustering, and unsupervised learning for static data labeling are its three branches. RL continuously interacts with the environment to generate actions based on state observations and rewards [26].

4.8 Test system with presence of the controller

In Figure 29, the test system is the two-area IEEE9 bus system (obtained from integration with RES in section 4.6.3 of this thesis), shown with the previously placed PMUs (blue circles in the Figure) from the earlier chapter, which includes Zero Injection Buses (ZIBs). The controller, installed at the solar PV plant and designed to reducing oscillations. Power System Stabilizers (PSSs) are taken out of the system to see how the controller affects damping oscillations and filters out other effects. In order to damp out low-frequency oscillations a Deep Deterministic Policy Gradient (DDPG-based) reinforcement learning control is presented. Additionally, to quickly correct the supplied action, the controller makes use of two error signals. The methodology covered in [26] were applied in this thesis regarding applying controller.

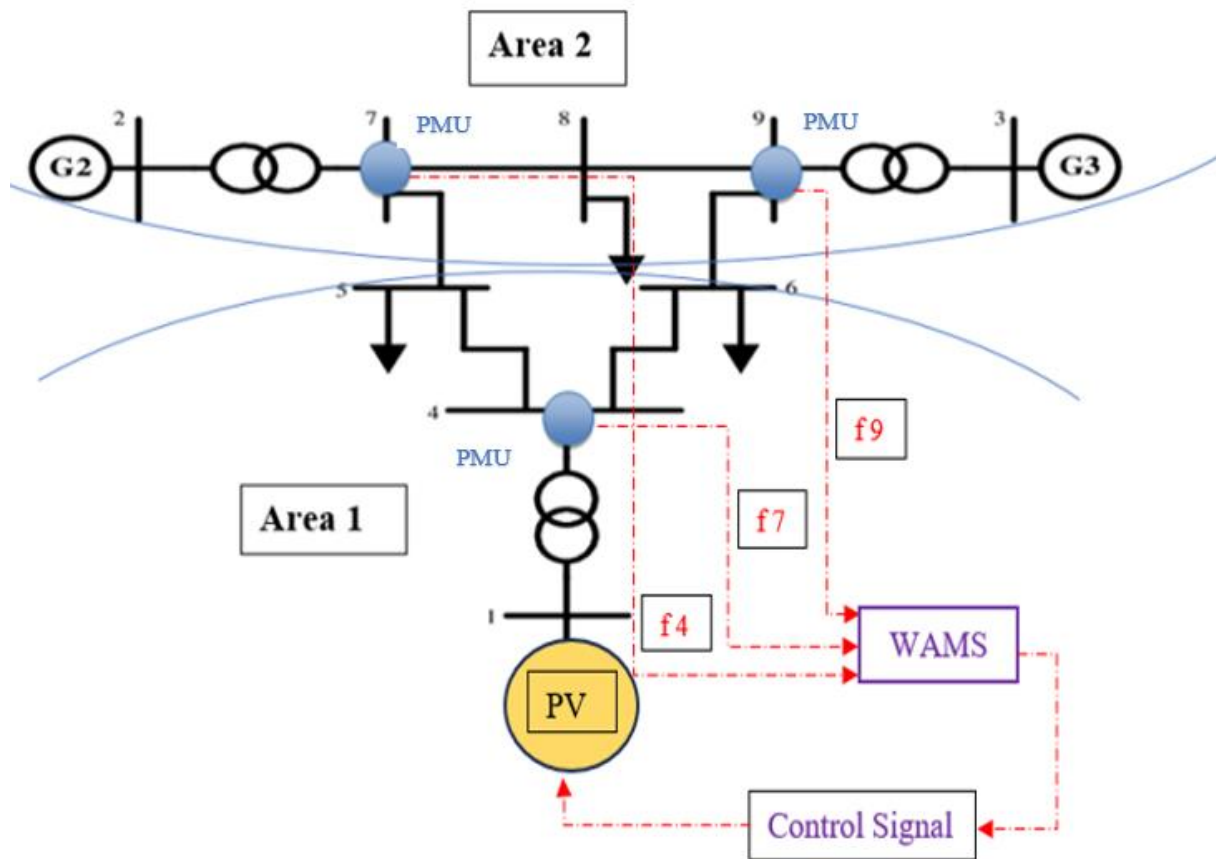


Figure 29- Test system with controller along with integrating PMUs and solar PV plant

4.9 Scheme for Reinforcement-Learning (RL) Control

Adaptive or optimum control techniques are frequently used by designers in traditional feedback control. The main difference is that adaptive control does not optimize parameters; instead, it modifies them in real-time based on available data. In contrast, optimal control requires dynamic system modeling and uses a mathematical model to adjust parameters offline. Reinforcement Learning (RL) is a machine-learning technique that creates adaptive and optimizing controllers without the need for system modeling by using input-output data from the system. Data learning is used to fine-tune the parameters. The two primary parts of RL are the environment and the agent. The controller to be designed is the agent. The environment, or system plant, is the whole system with the controller excluded. A closed loop is created by the two directed signals that link the agent and environment: (1) an outgoing signal that represents the controller action from the agent to the environment (2) Two more outgoing signals from the environment are sent to the agent, which adds a reward function signal to the plant's output and interprets it as an observation state (feedback signal). Over time, the reward signal improves

the caliber of the agent's behaviors. The agent consists of two neural network components: the actor and the critic. The goal is to maximize the amount of information learnt about the behavior of the system by optimizing its parameters, namely its weights and biases [26]. The Simulink version of above description is shown in Figure 30.

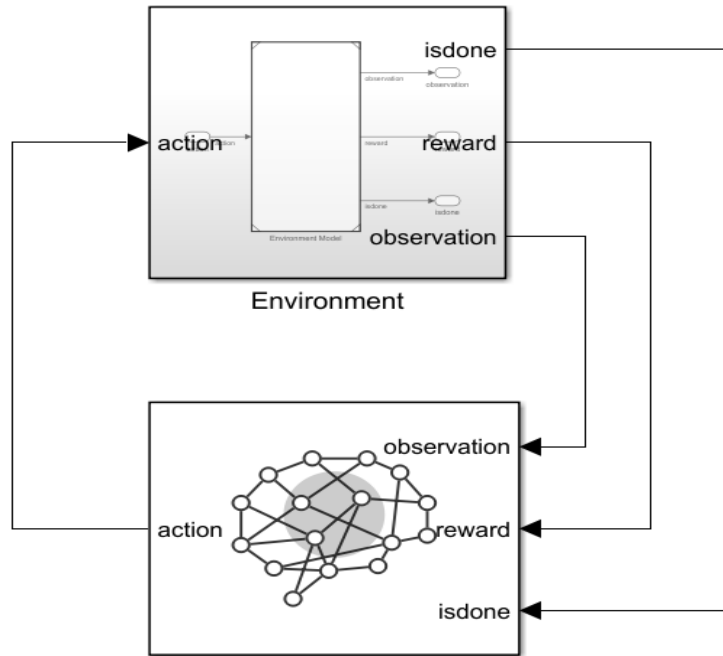


Figure 30- An agent-environment model in Simulink

The agent determines the controller's final policy by utilizing a method similar to the DDPG. The actor model in this algorithm takes a state as input and generates an action, recommending actions based on the state. The critic model is used by the agent which is also referred to as a learner, controller, or decision maker. In this model, the output is the Q-value, and the inputs are state and action. The quality of the actor's suggested behaviors is assessed by this Q-value (The Q-value is the action-value function and formally, for a state (s) and an action (a), is denoted as $Q(s, a)$). The critic is known as the policy evaluator or Q-function, while the actor is also called the behavior-function or policy maker. The structure of the RL system, encompassing the setup of the RL agent, observation signals, reward function, actor-critic network, training configurations, and environmental setup, is comprehensively detailed in [26] and data setting related to RL approach is available in [44].

4.9.1 RL Setup

4.9.1.1 RL agent setup

This thesis suggests using a remote signal from a WAMS to create an RL-based controller that efficiently dampens low frequency oscillations. To improve comprehension of these

oscillations, the agent acts in response to certain data, referred to as observation states. Since machine frequency data from PMUs is a critical indicator that is sensitive to system changes, the total of the measurements from each area is used to calculate the Center-Of-Inertia (COI) difference between areas. The Simulink configuration for the whole system is shown in Figure 31. The configuration of observation signal, reward function, actor-critic network, and training protocol are maintained consistently with the methodologies outlined in reference [26].

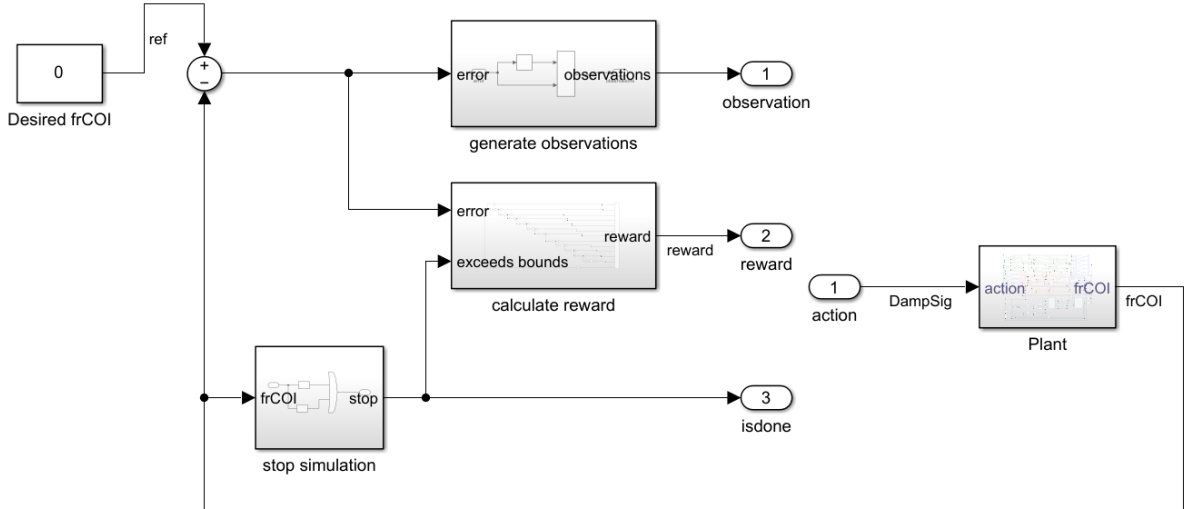


Figure 31- Simulink-based agent-environment control scheme

4.9.1.2 Environment Setup

Low frequency oscillations are a problem in the environment (plant) that the agent (controller) is intended to manage. The environment (plant) is the power system (IEEE-9 bus system as the test system) which is available in PSDAT package, with the agent excluded. The machines used in this thesis have turbine and exciter systems installed and the detailed sixth-order model of the generator is used. As discussed earlier in section 4.3, the Differential-Algebraic Equations (DAEs) that represent the system mathematically are presented together with the computation of the initial conditions for each variable and state.

4.10 Simulation Results (With RL controller)

In this thesis's last section, an effort was made to use the Deep Deterministic Policy Gradient (DDPG) algorithm to create the RL-based controller that was previously addressed. A PV power plant was installed in place of one of the conventional generators (G1) in the area 1 of the IEEE 9-bus test system, which was modified to reflect the move toward renewable energy

sources. Renewables (here Solar PV plant) do not naturally produce damping through mechanical inertia like conventional power plants do. Integrating the RL-based controller can compensate for this by providing necessary damping effects. The RL controller's performance was evaluated by focusing on its ability to dampen low-frequency oscillations (in section 4.6.3 of thesis) following system disturbance. It should be noted that all Power System Stabilizers (PSSs) were removed to isolate the effects of the RL controller on damping oscillations. After a disturbance was introduced at $t = 2$ seconds, the RL controller was simulated for 20 seconds. The frequency responses of generators G2 and G3 are depicted in Figure 32.

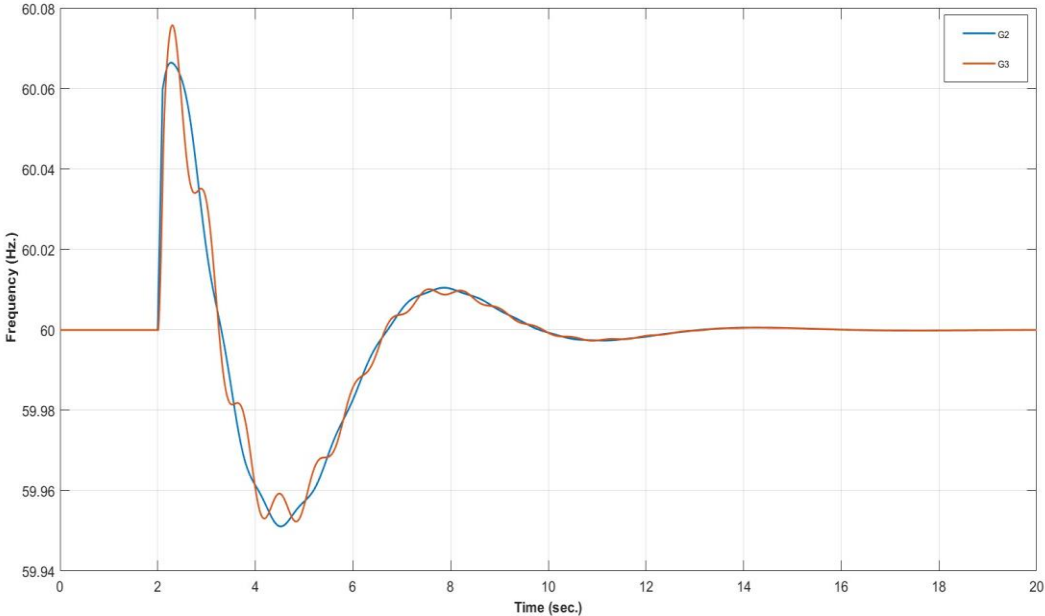


Figure 31- System analysis with RL controller in time domain

As time progresses, Figure 32 shows a damping of oscillations, indicating that the frequency is returning toward the nominal value (60 Hz). This dampening effect showcases the efficacy of the implemented RL-based controller, which actively damps out the oscillations and restore system stability. The frequency stabilizes around 60 Hz by $t = 14$ seconds, demonstrating the controller's role in maintaining system frequency within acceptable limits after disturbances.

The results show that the RL controller can stabilize the system frequency and attenuate oscillations in an adaptive manner. The RL controller was supposed to learn the best course of action to minimize system instability following a disturbance, and this behavior is consistent with the theoretical predictions covered in Section 4.9.

5. Conclusion and Recommendations for Future Work

5.1 Summary of Key Findings

In order to improve power system stability, this thesis investigated the integration of Phasor Measurement Units (PMUs) for optimal observability and the use of Wide Area Control (WAC) techniques based on Reinforcement Learning (RL). The two main goals of the thesis were to: (1) optimize PMU placement using the Connectivity Matrix Algorithm (CMA) to achieve comprehensive system observability; and (2) implement and assess a controller based on Reinforcement Learning (RL) intended to stabilize power systems dynamically, particularly those integrating Renewable Energy Sources (RES). Key findings include:

PMU Placement: The CMA was successful in identifying the optimal locations for PMUs, which improved system observability in a range of different IEEE bus configurations.

RL-Based Control Strategy: The results of the simulation showed that, the RL controller efficiently reduces oscillations and preserves system stability. This is particularly crucial in systems with high Renewable Energy Resources (RESs) penetration, which are inherently more volatile due to the fluctuating nature of renewable energy.

5.2 Limitations and Challenges

The primary obstacle faced during this study were mostly:

1-Simulation Constraints: The RL-based techniques were evaluated in simulated settings that might not accurately represent the complexities of real power systems.

2-Integration of Renewable Energy: The proposed RL controller only partially addressed the continuous challenges to system stability and control posed by the variability and unpredictability of renewable energy sources.

3-Scalability and Generalization: More research is needed to see whether the suggested solutions can be extended to wider and more varied networks.

5.3 Recommendation for Future Work

Future studies should concentrate on resolving the issues raised in this thesis by:

1-Advanced RL Algorithms: Create and evaluate more complex RL algorithms that are capable of adapting to the changing conditions of power systems that have a high degree of RES integration.

2-Scalability Studies: To ensure the efficacy and resilience of the suggested approaches on a larger scale, examine their use over more expansive network topologies, such as larger IEEE bus systems. Understanding the complexities and difficulties of implementing PMU and RL-based control techniques at a national or continental scale will be aided by expanding the experiments to incorporate larger and more complicated networks.

3-Improvements in Cybersecurity: With the growing dependence on digital and remote technologies, strengthening cybersecurity defenses will be essential to shielding power systems against emerging threats.

4-Consideration of Power System Stabilizers (PSSs): Exploring the combined use of PSSs and Reinforcement Learning (RL)-based controllers or any other advanced controllers, ensuring that PSSs are not removed during integration, to enhance the overall stability and robustness of the power system.

References

- [1] S. Chakrabarti, E. Kyriakides, and D. G. Eliades, "Placement of Synchronized Measurements for Power System Observability," *IEEE Transactions, Power Delivery*, vol. 24, pp. 12-19, 2009.
- [2] Jyoti Paudel, "Phasor Measurement Unit Deployment Approach for Maximum Observability Considering Vulnerability Analysis" Clemson university, Master Thesis 2015.
- [3] A. G. Phadke, "Synchronized phasor measurements in power systems," *IEEE Computer Applications in Power*, vol. 6, pp. 10-15, 1993.
- [4] A. G. Phadke and J. S. Thorpe, "Synchronised Phasor Measurements and Their Applications", *Power Electronics and Power Systems*, Springer 2008.
- [5] G. Missout and P. Girard, "Measurement of Bus Voltage Angle Between Montreal and SEPT-ILES," *IEEE Transactions, Power Apparatus and Systems*, vol. PAS-99, pp. 536-539, 1980.
- [6] N. Ashby, D. Allan, C. Hodge, "The Science of Timekeeping," Hewlett Packard Application Note 1289, 1997.
- [7] S. Soni, S. Bhil, D. Mehta, S. Wagh, "Linear state estimation model using phasor measurement unit (PMU) technology", *Electrical Engineering, Computing Science and Automatic Control (CCE)*, 2012 9th International Conference, pp 1–6, Sep. 2012.
- [8] P. Overholt, D. Ortiz and A. Silverstein, "Synchro-phasor Technology and the DOE: Exciting Opportunities Lie Ahead in Development and Deployment," in *IEEE Power and Energy Magazine*, vol. 13, no. 5, pp. 14-17, Sept.-Oct. 2015.
- [9] J. E. Dagle, "The North American Synchro Phasor Initiative (NASPI)," *IEEE PES General Meeting*, Minneapolis, MN, USA, 2010, pp. 1-3.
- [10] W. Sattinger, "Application of PMU measurements in Europe TSO approach and experience," 2011 *IEEE Trondheim PowerTech*, Trondheim, Norway, 2011, pp. 1-4.
- [11] V. Terzija, P. Crossley, D. Novosel, D. Karlsson, H. Li, presentation of WAMPAC course, Manchester, UK, July 2007.
- [12] N. M. Manousakis, G. N. Korres, and P. S. Georgilakis, "Taxonomy of PMU Placement Methodologies," *IEEE Transactions, Power Systems*, vol. 27, pp. 1070- 1077, 2012.

- [13] Amer Al-Hinai, AliReza Karami-Horestani, Hassan Haes Alhelou, A multi-objective optimal PMU placement considering fault-location topological observability of lengthy lines: A case study in OMAN grid, *Energy Reports*, Volume 9, 2023, Pages 1113-1123, ISSN 2352-4847.
- [14] Observability of power systems with optimal PMU placement Margarida Carvalho, Xenia Klimentova, Ana Viana, *Computers & Operations Research*, Volume 96, August 2018, Pages 330-349.
- [15] Cyber-attacks on PMU placement in a smart grid: Characterization and optimization Weiyong Ding, Maochao Xu, Yu Huang, Peng Zhao, Fengyi Song, *Reliability Engineering & System Safety*, Volume 212, August 2021, 107586.
- [16] A novel comprehensive optimal PMU placement considering practical issues in design and implementation of a wide-area measurement system: Moossa Khodadadi Arpanahi, Roozbeh Torkzadeh, Arash Safavizadeh, Ali Ashrafzadeh, Fariborz Eghtedarnia; *Electric Power Systems Research*; Volume 214, Part B, 15 January 2023, 108940.
- [17] Babu, R., Gupta, V.K. & Subbaramaiah, K. An Approach to Unravel the Optimal PMU Placement Problem for Full Observability of Power Network in View of Contingencies. *Int J Syst Assur Eng Manag* 13, 1170–1186 (2022).
- [18] Multi-Objective PMU Allocation for Resilient Power System Monitoring; 2020 IEEE Power & Energy Society General Meeting (PESGM), Haggi, Hamed; Sun, Wei; Qi, Junjian.
- [19] Weijun Lin, Qingbin Wang, Jingwei Long, Zizhuo Lian, Haoxian Liang, Zhilin Liang, "Optimization method of PMU placements base on costs and risk assessments of state estimation", *Energy Reports*, Volume 9, Supplement 12, 2023, Pages 348-355.
- [20] A.S. Musleh, S.M. Muyeen, A. Al-Durra, I. Kamwa, M.A.S. Masoum, S. Islam "Time-delay analysis of wide-area voltage control considering smart grid contingences in a real-time environment IEEE" *Trans. Industr. Informat.*, 14 (3) (2018), pp. 1242-1252.
- [21] A. Ashok, M. Govindarasu and J. Wang, "Cyber-Physical Attack-Resilient Wide-Area Monitoring, Protection, and Control for the Power Grid," in *Proceedings of the IEEE*, vol. 105, no. 7, pp. 1389-1407, July 2017.
- [22] S. Azizi, A. S. Dobakhshari, S. A. Nezam Sarmadi, and A. M. Ranjbar, "Optimal PMU Placement by an Equivalent Linear Formulation for Exhaustive Search," *IEEE Transactions, Smart Grid*, vol. 3, pp. 174-182, 2012.

- [23] M. Esmaili, K. Gharani, and H. A. Shayanfar, "Redundant Observability PMU Placement in the Presence of Flow Measurements Considering Contingencies," *IEEE Transactions, Power Systems*, vol. 28, pp. 3765-3773, 2013.
- [24] Roy, BK Saha, A. K. Sinha, and A. K. Pradhan. "An optimal PMU placement technique for power system observability." *International Journal of Electrical Power & Energy Systems* 42.1 (2012): 71-77.
- [25] C. Lu, Z. Wang, M. Ma, R. Shen and Y. Yu, "An Optimal PMU Placement with Reliable Zero Injection Observation," in *IEEE Access*, vol. 6, pp. 54417-54426, 2018
- [26] Abdulrahman, I. Reinforcement-learning-based damping control scheme of a PV plant in wide-area measurement system. *Electr Eng* 104, 4213–4225 (2022).
- [27] Cui, Q.; Kim, G.; Weng, Y. Twin-Delayed Deep Deterministic Policy Gradient for Low-Frequency Oscillation Damping Control. *Energies* 2021, 14, 6695.
- [28] Abdulrahman, I., Belkacemi, R. & Radman, G. Power oscillations damping using wide-area-based solar plant considering adaptive time-delay compensation. *Energy Syst* 12, 459–489 (2021).
- [29] Al-Momani, Mohammad M., et al. "Modified Connectivity Matrix Algorithm." 2022 *Advances in Science and Engineering Technology International Conferences (ASET)*, IEEE, 2022.
- [30] Al-Odienat, A. I., et al. "Connectivity Matrix Algorithm: A New Optimal Phasor Measurement Unit Placement Algorithm." *IOP Conference Series: Earth and Environmental Science*, vol. 551, no. 1, IOP Publishing, Aug. 2020, p. 012008.
- [31] B. Gou, "Optimal placement of PMUs by integer linear programming", *IEEE Transactions on Power Systems*, vol. 23, no. 3, pp 1525–1526, Aug. 2008.
- [32] R. F. Nuqui and A. G. Phadke, "Phasor measurement unit placement techniques for complete and incomplete observability," in *IEEE Transactions on Power Delivery*, vol. 20, no. 4, pp. 2381-2388, Oct. 2005.
- [33] I. Abdulrahman, "PSDAT Manual", Ver 1.0, Cookeville, TN, USA, 2019.
- [34] P. Sauer, M. A. Pai and J. H. Chow, *Power System Dynamics and Stability*, Hoboken, NJ, USA:Wiley, 2017.

- [35] W. Xu, E. Vaahedi, Y. Mansour, and J. Tamby, "Voltage stability load parameter determination from field tests on BC Hydro's system," *IEEE Trans. Power Syst.*, vol. 12, no. 3, pp. 1290–1297, Aug. 1997.
- [36] R. D. Zimmerman, C. E. Murillo-Sanchez, and R. J. Thomas, "MATPOWER: Steady-state operations, planning and analysis tools for power systems research and education," *IEEE Trans. Power Syst.*, vol. 26, no. 1, pp. 12–19, Feb. 2011.
- [37] B. Chaudhuri and B. Pal, *Robust Control in Power Systems*. New York, NY, USA: Springer, 2005.
- [38] P. Anderson and A. Fouad, *Power System Control and Stability*, 2nd ed. New Delhi, India: Wiley, 2003.
- [39] P. Kundur, *Power System Stability and Control*. New York: McGraw-Hill, 1994.
- [40] N. Hatziargyriou et al., "Definition and Classification of Power System Stability – Revisited & Extended," in *IEEE Transactions on Power Systems*, vol. 36, no. 4, pp. 3271–3281, July 2021.
- [41] P. Kundur et al., "Definition and classification of power system stability IEEE/CIGRE joint task force on stability terms and definitions," *IEEE Transactions on Power Systems*, vol. 19, no. 3, pp. 1387–1401, Aug. 2004.
- [42] Abdulrahman, I. An open-source Simulink-based program for simulating power systems integrated with renewable energy sources. *Electr Eng* 102, 2181–2192 (2020).
- [43] Xie, R., Kamwa, I., Rimorov, D., et al.: 'Fundamental study of common mode small-signal frequency oscillations in power systems', *Int. J. Electr. Power Energy Syst.*, 2019, 106, pp. 201–209.
- [44] Ismael Abdulrahman (2024). Reinforcement-Learning Based Damping Control Scheme of a PV (<https://www.mathworks.com/matlabcentral/fileexchange/124525-reinforcement-learning-based-damping-control-scheme-of-a-pv>), MATLAB Central File Exchange. Retrieved May 13, 2024.

